Gamma-cycle duration predicts instantaneous amplitude, spike rate and synchrony in macaque V1.

Georgios Spyropoulos,[1] Jarrod Robert Dowdall,[1,2] Marieke Louise Schölvinck,[1] Conrado Arturo Bosman,[3,4] Bruss Lima,[5,6] Alina Peter,[1,2] Irene Onorato,[1,2] Johanna Klon-Lipok,[1,5] Rasmus Roese,[1] Sergio Neuenschwander,[5,7] Wolf Singer,[1,5,8] Martin Vinck,[1,9] Pascal Fries[1,3,9,10,*]

[1]Ernst Strüngmann Institute (ESI) for Neuroscience in Cooperation with Max Planck Society, 60528 Frankfurt, Germany

[2]International Max Planck Research School for Neural Circuits

[3]Donders Institute for Brain, Cognition and Behaviour, Radboud University, 6525 EN Nijmegen, the Netherlands

[4]Swammerdam Institute for Life Sciences, Center for Neuroscience, Faculty of Science, University of Amsterdam, 1098 XH Amsterdam, the Netherlands

[5]Max Planck Institute for Brain Research, 60438 Frankfurt, Germany

[6]Carlos Chagas Filho Institute of Biophysics, Federal University of Rio de Janeiro, 21941-902 Rio de Janeiro, Brazil

[7]Brain Institute, Federal University of Rio Grande do Norte, 59056-450 Natal, Brazil

[8]Frankfurt Institute for Advanced Studies, 60438 Frankfurt, Germany

[9]These authors contributed equally to this work

[10]Lead Contact

*Correspondence: pascal.fries@esi-frankfurt.de

Spyropoulos et al., Gamma-cycle amplitude versus duration in macaque visual cortex

SUMMARY

Communication among visual cortical areas depends on gamma oscillations. Respective gamma cycles vary substantially in amplitude and duration, yet it is unclear how those fundamental parameters relate to each other and to spiking activity. We recorded local-field-potentials (LFPs) and spiking activity from awake macaque area V1 and detected amplitude, duration and spiking activity per gamma cycle. Longer durations predicted larger amplitudes and stronger spike synchrony, yet lower spike rates. These findings suggest that spontaneous gamma-variability reflects inhibitory mechanisms that reduce spike rates, increase synchronization, and prolong the cycle duration. The classical LFP power-spectrum, estimated on longer time scales, was most strongly predicted from *how often* certain gamma-cycle durations occurred, rather than by their associated instantaneous amplitudes.

INTRODUCTION

Gamma oscillations are a prominent feature of the activated cortex and likely contribute to stimulus processing (Cardin et al., 2009; Gray et al., 1989; Siegle et al., 2014), interareal communication (Bosman et al., 2012; Buschman and Miller, 2007; Colgin et al., 2009; Gregoriou et al., 2009; Grothe et al., 2012; Rohenkohl et al., 2018; Womelsdorf and Fries, 2007), attention (Bichot et al., 2005; Fries et al., 2001), spatial memory (Bieri et al., 2014; Zheng et al., 2016) and working memory (Pesaran et al., 2002). Many aspects of the gamma rhythm are, nevertheless, poorly understood. In particular, assumptions concerning its stationarity are often violated. Recent work suggests that gamma amplitude and frequency fluctuate considerably over time (Burns et al., 2011; Lowet et al., 2018; Lowet et al., 2016; Lundqvist et al., 2016) and cortical space (Lima et al., 2010; Lowet et al., 2017; Ray and Maunsell, 2010). This is particularly important for theories that implicate gamma rhythms in interareal communication (Akam and Kullmann, 2012; Fries, 2015; Palmigiano et al., 2017).

The non-stationary character of gamma oscillations is a consequence of the network mechanism of gamma generation. An influential network model of gamma, the pyramidal interneuronal network gamma (PING) model posits that gamma originates from the interplay of excitation and inhibition (Börgers and Kopell, 2003; Buzsáki and Wang, 2012; Tiesinga and Sejnowski, 2009; Tiesinga et al., 2001; Traub et al., 1997; Whittington et al., 2000). The interaction of excitation and inhibition is, itself, a ubiquitous feature of cortical circuits, and is highly non-linear. Specifically, the amount of excitation in a given gamma cycle should determine the duration of the subsequent inhibition: Stronger bouts of excitation should lead to gamma cycles of larger amplitude, which should be followed by longer inhibition and correspondingly longer gamma cycle duration (Okun and Lampl, 2008; Shu et al., 2003; Traub et al., 1996; Wehr and Zador, 2003; Whittington et al., 1995). The predicted positive correlation between gamma cycle amplitudes and durations has actually been reported in rodent hippocampus (Atallah and Scanziani, 2009).

The rodent hippocampus has been the main model system from which empirical support for the PING model derives (Atallah and Scanziani, 2009; Bragin et al., 1995; Csicsvari et al., 2003;

Spyropoulos et al., Gamma-cycle amplitude versus duration in macaque visual cortex

61 Mann et al., 2005). Another prominent model system, in which gamma oscillations have been
62 extensively studied, is primate visual cortex, and particularly macaque area V1. Here, much
63 work has been devoted to gamma synchronization between V1 and higher areas V2 and V4, its
64 role in interareal communication and its modulation by attention (Bastos et al., 2015; Bosman et
65 al., 2012; Grothe et al., 2012; Jia et al., 2013a; Lowet et al., 2018; Lowet et al., 2016; Roberts et
66 al., 2013; Rohenkohl et al., 2018). If in this system, too, gamma-cycle amplitudes and durations
67 were correlated, this could provide an important link to models of gamma that are based on
68 rodent electrophysiology. A mechanistic relationship between instantaneous gamma-cycle
69 amplitude and duration may also contribute to the emergence of gamma synchronization: A
70 strong, synchronous bout of excitation in a pre-synaptic group of neurons could induce a long
71 gamma-cycle both in this pre-synaptic and a post-synaptic group, due to subsequent inhibition.
72 This would lead to coherent fluctuations in instantaneous frequency between these two
73 neuronal groups and thereby aid their gamma synchronization. This mechanisms could be at
74 play both within (Lowet et al., 2017) and between (Roberts et al., 2013) areas.

75 There is some evidence that gamma synchronization in awake macaque V4 is generated by an
76 excitatory-inhibitory balance, similar to rodent hippocampus (Vinck et al., 2013a). However, the
77 evidence for the relation between gamma amplitude and frequency, i.e. the inverse of the
78 gamma cycle duration, so far suggests no consistent relationship (Jia et al., 2013b). Many
79 recent studies in macaques, primarily in V1, have identified a multitude of contextual and top-
80 down factors that influence the amplitude and frequency of gamma oscillations. The amplitude
81 and/or frequency of gamma are known to be modulated by visual contrast (Jia et al., 2013b;
82 Ray and Maunsell, 2010; Roberts et al., 2013), the relation between stimulus orientation and
83 neuronal orientation preference (Jia et al., 2013b; Lima et al., 2010), the size of visual stimuli
84 (Gieselmann and Thiele, 2008; Peter et al., 2019), stimulus repetition (Brunet et al., 2014), time
85 after stimulus onset (Jia et al., 2011), eye movements (Bosman et al., 2009; Lowet et al., 2016),
86 and attention (Bosman et al., 2012). Some of these factors enhance both gamma amplitude and
87 frequency, whereas some enhance one of them and reduce the other. For example, the size of
88 visual stimuli is positively correlated with the amplitude and negatively correlated with the
89 frequency of gamma (Gieselmann and Thiele, 2008; Peter et al., 2019), in accordance with the
90 findings reported in rodent hippocampus (Atallah and Scanziani, 2009). However, the contrast
91 of visual stimuli is positively correlated with both gamma amplitude and frequency (Jia et al.,
92 2013b; Ray and Maunsell, 2010; Roberts et al., 2013). Thus, while some stimulus factors lead
93 to positive correlations between gamma cycle amplitudes and durations, compatible with the
94 abovementioned evidence from rodents, others lead to negative correlations.

95 The stimulus factors outlined above do not exclude the possibility that the fundamental
96 mechanism of gamma generation in awake macaque visual cortex produces a positive
97 correlation between gamma-cycle amplitudes and durations. We addressed this question by
98 recording local-field-potentials (LFPs) and spiking activity from awake macaque area V1. We
99 developed a method to detect the amplitude and duration per gamma cycle, which circumvented
100 major problems of previous methods and allowed us to analyze the relationship of a gamma-
101 cycle's duration with its amplitude, and with spike rates and spike-field coherence.

Spyropoulos et al., Gamma-cycle amplitude versus duration in macaque visual cortex

RESULTS

102

103 We recorded local field potentials (LFPs) and spiking activity from primary visual cortex (V1) of
104 several macaque monkeys (see Methods). The monkeys performed a fixation task, while drifting
105 gratings or uniform color surfaces were presented. Figure 1A shows an example trial of
106 broadband LFP recorded during the presentation of a full-screen drifting grating. The trial-
107 average spectra of absolute power (Figure 1B) and of power change relative to pre-stimulus
108 baseline (Figure 1C) reveal very strong visually induced gamma oscillations. The time-
109 frequency analysis (Figure 1D) shows that this induced gamma is sustained for the duration of
110 stimulation. Figure 1F-I shows similar results for visual stimulation with a colored surface (Peter
111 et al., 2019; Shirhatti and Ray, 2018).

112 For these data, we investigated the relationship between gamma-cycle amplitude and duration.
113 We first performed this analysis in a way that followed as closely as possible the approach used
114 by (Atallah and Scanziani, 2009) for data from awake freely-moving rats. One difference was
115 that we focused on the visual stimulation period, whereas Atallah and Scanziani used the
116 ongoing LFP during anesthesia or wakefulness. In short, LFP signals were band-pass filtered
117 effectively between 20 and 100 Hz (Figure 2A; see Methods for details), and LFP segments that
118 had relatively high power in the gamma-frequency range were selected. For these selected LFP
119 segments, gamma peaks and troughs were identified as, respectively, the local maxima and
120 minima of the filtered LFP. The cycle amplitude was determined as the voltage difference
121 between each peak and its subsequent trough, and the cycle duration as the interval between
122 each peak and its subsequent peak (Figure 2B). For each gamma cycle, we thus obtained two
123 values, namely the cycle amplitude and the cycle duration. For each LFP channel separately,
124 we then computed the Pearson correlation coefficient between same-cycle amplitude and
125 duration values, across all gamma cycles detected for a given recording site in a given dataset
126 (see Methods) (Figure 2C, red bars). In addition, the correlation coefficient was computed
127 between the amplitude of a given cycle and the duration of the preceding cycle (Figure 2C,
128 white bars left of red bars), and also between the amplitude of a given cycle and the duration of
129 the succeeding cycle (Figure 2C, white bars right of red bars). We averaged these correlations
130 across recording sites within a given dataset. Across datasets, the correlation between the
131 amplitude and duration of the same cycle was significantly positive (Figure 2C red bars; $p < 5*10^{-5}$,
132 t-test; $p < 0.05$, two-sided non-parametric permutation test across datasets), whereas the
133 correlations between the amplitude of one cycle and the duration of either the preceding or
134 succeeding cycle were not significant (Figure 2C white bars for preceding cycle: $p = 0.28$, t-test;
135 white bars for succeeding cycle: $p = 0.56$, t-test; for both cases $p > 0.05$, two-sided non-parametric
136 permutation test across datasets). We repeated those analyses for the Spearman instead of the
137 Pearson correlation and found those values to be almost identical, which is in agreement with
138 (Atallah and Scanziani, 2009).

139 We wondered whether cycle amplitude and duration were also correlated during the pre-
140 stimulus baseline period. During this period, there was no detectable gamma peak in the LFP
141 power spectrum, but rather a characteristic $1/f^n$ trend in the gamma-frequency range

Spyropoulos et al., Gamma-cycle amplitude versus duration in macaque visual cortex

142   (Figures 1B and 1G). Nevertheless, the analysis method used above (Atallah and Scanziani,
143   2009) resulted in the detection of a substantial number of "gamma cycles", i.e. cycles with an
144   instantaneous frequency in the gamma range. We did not expect that for this period, the
145   correlation between gamma-cycle duration and amplitude would be as strong as for the visual
146   stimulation period, in which gamma oscillations were very strong. To our surprise, the
147   correlation between cycle amplitude and duration in the pre-stimulus period was in fact higher
148   than in the visual stimulation period (Figure 2D red bars; $p<5*10^{-5}$, t-test). A sufficiently long pre-
149   stimulus period was available in only a subset of the datasets, yet the correlation was higher for
150   each of them. Thus, a very strong correlation between cycle-by-cycle amplitude and duration
151   existed in the absence of a detectable gamma peak, when using the same approach as
152   previously used in rodent hippocampus (Atallah and Scanziani, 2009).

153   It is conceivable that in the baseline period, fluctuations in the gamma-frequency range reflect a
154   rhythmic gamma component that remains undetected in the power spectrum. We therefore
155   investigated the relationship between gamma-cycle amplitude and duration for the case of
156   synthetic noise signals, in which no rhythmic gamma component is present. We generated
157   synthetic noise signals having a power spectrum with a $1/f^n$ shape, where n ranged between 0
158   (white noise) and 2 (Brownian noise) (Figure 2F). We then analyzed these signals with the
159   same method as used for the LFP signals, and observed a highly significant positive correlation
160   between the amplitude and duration of individual deflections in the gamma-frequency range.
161   The magnitude of this correlation increased as a function of the $1/f^n$ slope of the underlying
162   power spectrum (Figure 2G). Thus, noisy fluctuations in a signal without rhythmic components
163   can give rise to a strong positive correlation between the amplitude and duration of "gamma-
164   cycles". Note that in this case, the "gamma rhythmicity" is due to band-pass filtering (Figure 2E).
165   This relationship should hold even for a random-walk process, where the magnitudes of
166   successive steps (i.e. increments or decrements in the signal) are independent of each other
167   and follow a normal distribution with zero mean. In this case, any reversal of direction will
168   produce a peak or a trough. The peak-to-trough distance defines the duration of a "cycle" as the
169   number of steps. The greater this number, the greater the expected amplitude of the respective
170   "cycle", because it is composed of a larger number of steps in the same direction, and because
171   steps in a given direction are always drawn from the same distribution, namely the positive or
172   negative half of the normal distribution.

173   To address this problem, we developed a different method to detect the instantaneous
174   amplitude and duration of a gamma cycle (Figure 3, see Methods for details). This method was
175   designed to prevent the detection of peaks and troughs due to noisy fluctuations. In addition, it
176   was designed to circumvent problems related to band-pass filtering. Specifically, band-pass
177   filtering creates dependencies between voltage values across time points, and can transform
178   transient, non-oscillatory deflections into rhythmic events. The first step of our method was to
179   compute the Hilbert transform on the broadband LFP-signal (i.e. without band-pass filtering in
180   the gamma-frequency range). Based on the Hilbert transform, we extracted the phase of the
181   analytic signal (Figure 3B) and computed the first temporal derivative of the unwrapped phase
182   to obtain the angular velocity (Figure 3C). Data segments that contained an angular velocity

Spyropoulos et al., Gamma-cycle amplitude versus duration in macaque visual cortex

183 below zero (phase slips) were excluded from further analysis. The absence of such phase slips
184 and thereby the presence of a stable positive angular velocity suggests that the signal is
185 dominated by one rhythm. In the visual stimulation period, we detected many data segments
186 fulfilling this criterion, and the dominating rhythm was in the gamma-frequency range
187 (Figures 3A-3C). By contrast, very few segments were detected in the pre-stimulus period. We
188 then used the analytic signal to determine the peaks and troughs of the gamma cycles.
189 Specifically, we identified gamma peaks by first detecting negative-to-positive zero crossings in
190 the phase of the analytic signal. For each of these crossings, we then identified the nearest local
191 maximum in the LFP signal (Figure 3D). Likewise, gamma troughs were identified by detecting
192 positive-to-negative zero crossings and identifying nearby local minima. Using the detected
193 gamma peaks and troughs, we then determined the gamma-cycle amplitude and duration. To
194 obtain estimates of gamma-cycle amplitude and duration with the maximum attainable temporal
195 resolution, we divided each gamma cycle into "half-cycles": The first half-cycle comprised the
196 data segment from the trough to the peak, and the second half-cycle from the peak to the
197 trough. For each half-cycle, amplitude was defined as the difference between the respective
198 peak and trough, and duration was defined as the corresponding time interval. For each
199 detected half-cycle, we thus obtained an amplitude and duration value. In summary, this revised
200 method avoided filtering in the gamma band and focused on data segments dominated by one
201 rhythm, which in our datasets was the gamma rhythm.

202 In addition, we aimed at excluding correlations between cycle amplitude and duration that could
203 be explained by external factors, like stimulation. Figures 1E and 1J illustrates such stimulus-
204 related correlation by showing time courses of gamma-cycle amplitudes (blue) and durations
205 (red) as a function of time after stimulus onset. For stimulation with a grating, amplitudes and
206 durations both increased with time. By contrast, for stimulation with a colored surface,
207 amplitudes decreased while durations increased. Such post-stimulus dynamics would lead to
208 substantial correlations, if correlations were calculated across all cycles, and the examples
209 show that these correlations could be positive or negative. We aimed at eliminating such
210 extrinsic effects, to isolate as much as possible the correlation between amplitude and duration
211 that is due to the fundamental mechanisms underlying gamma-rhythm generation. Therefore,
212 we computed correlations, across trials, separately for each time point after stimulus onset and
213 then averaged them over post-stimulus time (see Methods for details). We quantified the
214 correlation as the Spearman correlation coefficient, because this avoids assumptions about
215 underlying distributions and about the linearity of their relation, and was found to be similar to
216 the Pearson correlation in these data (see above) and the previous study (Atallah and
217 Scanziani, 2009). Using this approach, amplitudes and durations of gamma half-cycles were
218 positively correlated in all tested datasets (Figure 4A; red bars; p=0.006, t-test; p<0.05, two-
219 sided non-parametric permutation test across datasets). Note that the magnitude of these
220 correlations was, on average, substantially lower than the one observed with the previously
221 employed method. Thus, amplitude and duration were positively correlated for cycles of visually
222 induced gamma in the awake macaque, and this correlation was not due to noise, progressive
223 changes in gamma over time after stimulus onset, or band-pass filtering. These results are
224 consistent with the notion that similar mechanisms might underlie gamma rhythm generation in

Spyropoulos et al., Gamma-cycle amplitude versus duration in macaque visual cortex

225 awake macaque V1 and rodent hippocampus. In addition, we found no consistent pattern
226 across datasets in the correlation between the instantaneous amplitude of the current half-cycle
227 and the duration of the previous or the subsequent half-cycles (Figure 4A; white bars for
228 preceding cycle: p=0.5, t-test; white bars for succeeding cycle: p=0.35, t-test; for both cases
229 p>0.05, two-sided non-parametric permutation test across datasets). Similar results were
230 obtained for full rather than half cycles (Figure S1A; red bars; p=0.011, t-test; p<0.05, two-sided
231 non-parametric permutation test across datasets; white bars for preceding cycle: p=0.13, t-test;
232 white bars for succeeding cycle: p=0.9, t-test; for both cases p>0.05, two-sided non-parametric
233 permutation test across datasets).

234 The last paragraph aimed at excluding correlations due to slow (slower than cycle-by-cycle)
235 post-stimulus dynamics. Yet, such correlations might as well be due to other slow dynamics e.g.
236 due to drifts or slow oscillations in the monkey's state, or to stimulus repetition. We investigated
237 the influences of slower dynamics by computing correlation coefficients for up to ten preceding
238 and succeeding half-cycles (Figure 4B). Some datasets showed dynamics on the temporal
239 scale of few half-cycles (Figure 4B, left), others on the scale of multiple half-cycles (Figure 4B,
240 middle and right). For example, the right panel in Figure 4B shows a long-lasting negative trend
241 punctuated by a small positive value for the instantaneous correlation. By contrast, the middle
242 panel shows a positive trend peaking at zero lag. The potential sources of those longer-time-
243 scale correlations are manifold. This includes for the lagged correlations the post-stimulus
244 dynamics, but likely other unknown sources as well. There is no obvious way to remove them
245 explicitly, like we did for the influence of post-stimulus dynamics on the instantaneous
246 correlation. Therefore, we removed the influences of slower dynamics globally through a
247 regression analysis: As above, we first computed the half-cycle amplitude and duration for each
248 time point after stimulus onset. For each half-cycle, we then predicted the amplitude value of the
249 ongoing half-cycle from the amplitude values of the previous and next half-cycle, by using a
250 least squares approach (see Methods). We used the same procedure for half-cycle duration
251 values. This was done for each point after stimulus onset separately, and by using all the
252 amplitude and duration values across trials (for that time point). From these regression
253 analyses, we then obtained residual values of amplitude and duration for each half-cycle. These
254 residual values measured the extent to which the amplitude or duration in the ongoing half-cycle
255 was greater or smaller than in the surrounding half-cycles, and thereby departed from slower
256 trends. We then computed the correlation between the regression residuals for amplitude and
257 duration, in the same way as described above. On average across datasets, the resulting
258 correlation (Figure 4C; red bars; p=0.0023, t-test; p<0.05, two-sided non-parametric permutation
259 test across datasets) was comparable to the correlation between raw amplitude and duration
260 (Figure 4A). This indicates that it is unlikely that the positive correlation between gamma
261 amplitude and duration was due to within- or across-trial trends on a longer timescale. Rather,
262 this finding suggests that the correlation was due to cycle-by-cycle fluctuations in amplitude and
263 duration. Again, similar results were obtained for full rather than half cycles (Figure S1B; red
264 bars; p=0.008, t-test).

Spyropoulos et al., Gamma-cycle amplitude versus duration in macaque visual cortex

265   We performed an additional analysis to address the issue of non-stationary fluctuations over
266   longer time-scales or trials, by using an autoregressive (AR) model of the LFP data. An AR
267   model captures the variance and auto-correlation of the LFP and can then be used to generate
268   surrogate time series without non-stationary fluctuations in cycle amplitude and duration on a
269   slower time-scale. Figure S2 illustrates this for the dataset from Figures 1A-1E. The AR model
270   accurately captured the power spectrum (Figure S2B), but did not replicate slower dynamics in
271   gamma cycle amplitudes or durations (Figure S2C, D, compare to Figure 1D, E). We analyzed
272   the correlations between half-cycle amplitudes and durations in the surrogate data generated by
273   the AR model, and replicated the positive sign of the instantaneous correlation between half-
274   cycle amplitude and duration (Figure S2E; red bars; p=0.03, t-test). This further reinforces the
275   notion that the observed correlations were not due to co-fluctuations on a slower time-scale.
276   Again, similar results were obtained for full rather than half cycles (Figure S1C; red bars;
277   p=0.041, t-test).

278   Next, we investigated whether the correlation between half-cycle amplitudes and durations may
279   have been influenced by small saccadic eye-movements that occur during fixation
280   (microsaccades; MSs). These MSs can have a substantial impact on the amplitude and
281   frequency of visually induced gamma oscillations (Bosman et al., 2009; Lowet et al., 2018;
282   Lowet et al., 2016), which is also true in the datasets analyzed here (Figure 5A and 5B). It is
283   possible for example that after a MS, both, half-cycle amplitude and duration, show a transient
284   correlated change, which could result in either a positive or negative correlation between
285   amplitude and duration. To address this, we performed correlation analyses after excluding data
286   epochs between MSs and 250 ms thereafter. We performed the correlation analysis in the same
287   way as for Figure 4AC, i.e. after regressing out longer-term trends in amplitudes and durations.
288   Despite significant reductions in the amount of available data segments, we found that the
289   resulting correlations between half-cycle amplitude and duration remained significantly positive
290   in all examined datasets and in the average across datasets (Figure 5C; red bars; p=0.023, t-
291   test, see S1D for analysis with full cycles; red bars; p=0.043, t-test). This indicates that the
292   observed correlations between half-cycle amplitude and duration were not due to MS-related
293   non-stationarities. Based on the analyses presented in Figures 4, 5, and S1, we conclude that
294   half cycles with longer durations tend to have larger amplitudes.

295   The observed correlation was smaller than previously reported in rodent hippocampus (Atallah
296   and Scanziani, 2009), but remained robust when accounting for extrinsic factors that may have
297   obscured it. This correlation however does not necessarily imply a monotonic or linear
298   relationship between half-cycle amplitudes and durations, as was reported by Atallah and
299   Scanziani (2009). In order to examine this, we computed the average half-cycle amplitude for
300   each possible half-cycle duration (Figure 6, blue curves; see Methods). We call this the cycle-
301   based spectrum (CBS). For this and all following analyses, to minimize the aforementioned
302   influence of slow stimulus-locked trends in gamma amplitude and frequency, we only used the
303   final 250 ms of visual stimulation. To average CBSs across monkeys, we first converted half-
304   cycle duration values to frequency values (in Hz). We then aligned the CBSs to the "gamma
305   peak frequency" obtained from the conventional LFP power spectrum, i.e. the frequency at

8

306   which LFP gamma-band power reached a maximum. We did this separately for the gamma
307   peak frequency obtained from the raw power spectrum (Figure 6A) or the power change
308   spectrum (Figure 6B) to account for possible differences between them. We found that the
309   average CBS had the shape of an inverted U-curve: half-cycle amplitude showed a non-
310   monotonic relationship with frequency (i.e. inverse of duration); interestingly, amplitude was
311   greatest at a frequency that was lower than the peak gamma frequency and showed a decline
312   towards higher gamma frequencies.

313   We wondered how the shape of the CBS was related to the LFP power spectrum. We observed
314   that the LFP power spectrum was approximately symmetric and showed a steep decrease in
315   amplitude for frequencies below and above the peak gamma-frequency. Thus, the LFP power
316   spectrum had a markedly different shape than the CBS. In other words, the CBS and the
317   classical LFP power had a different dependence on frequency. This finding was surprising,
318   considering that one would expect that the LFP power spectrum measures the average
319   amplitude of oscillations at a given frequency. To understand this further, we considered that the
320   LFP power spectrum should be determined by two main factors: (1) The average cycle
321   amplitude as a function of a cycle's duration, and (2) how often different cycle durations, i.e. the
322   corresponding frequencies, tended to occur (henceforth referred to as "rate of incidence").
323   Because our analysis indicated that the shape of the LFP power spectrum is not well explained
324   by the first factor, we expected that the rate of incidence of cycle-by-cycle durations better
325   matches the shape of the LFP power spectrum. Indeed, we found that the rate of incidence of
326   gamma-cycle frequencies showed a better match to the LFP power spectrum (Figure 6, red
327   curves). Specifically, the most prevalent half-cycle frequency was found within one Hertz of the
328   peak gamma frequency derived from either the raw LFP power spectrum or the power change
329   spectrum. Thus, the LFP power spectrum was less informative about the amplitudes of the
330   underlying half-cycles, and more informative about how often a given half-cycle duration tended
331   to occur.

332   We wondered whether the observed dependency of amplitude on frequency was due to a
333   ceiling effect, considering that in our analysis, we selected LFP segments (using the broad-band
334   signal) in which gamma rhythms were relatively strong. This circumvented several
335   methodological problems, as discussed above, but may have limited the generalizability of our
336   findings. To address this issue, we re-analyzed the data after band-pass filtering the LFP in the
337   gamma-frequency range (20-100 Hz). This modification in our approach substantially increased
338   our sensitivity in detecting gamma episodes. The distributions of frequency and amplitude that
339   we obtained after band-pass filtering were, nevertheless, highly similar to the ones calculated on
340   the broad-band signal (Figures 6C and 6D). Thus, the specific distributions of frequency and
341   amplitude shown in Figures 6A and 6B were likely not a consequence of a ceiling effect.

342   The analyses above were restricted to LFP signals, which mostly reflect the synaptic potentials
343   in a population of neurons around the electrode. To gain deeper mechanistic insight, we next
344   asked how duration and amplitude of LFP gamma cycles were related to neuronal spiking
345   activity. The model of balanced excitation and inhibition, as it relates to the generation of

Spyropoulos et al., Gamma-cycle amplitude versus duration in macaque visual cortex

346 gamma oscillations, makes a specific prediction, namely that higher-amplitude gamma cycles
347 are initiated by a stronger bout of excitatory spiking (Atallah and Scanziani, 2009). These bouts
348 give rise to longer-lasting inhibition, resulting in longer gamma cycles. This, in turn, predicts the
349 presence of a negative correlation between neuronal firing rates and LFP gamma frequency,
350 which was reported for area CA3 of the rodent hippocampus (Atallah and Scanziani, 2009). In
351 order to assess if this prediction holds for awake macaque V1, we analyzed multi-unit (MUA)
352 activity along with LFPs recorded from area V1 in two macaques. Spiking activity was analyzed
353 in conjunction with gamma oscillatory epochs, which were extracted from the LFP using the
354 same general approach as described above (see Methods). For each MUA, we computed both
355 the normalized spike count (number of spikes per cycle) (Figure 7A) and the firing rate (number
356 of spikes per second) (Figure 7B) as a function of the cycle-by-cycle frequency, i.e. the inverse
357 of cycle-by-cycle duration (see Methods). The normalized spike count was negatively correlated
358 with the gamma-cycle frequency (Figure 7D, first pair of bars), which indicates that units fired
359 more spikes in cycles with a longer duration. Note that spike count per cycle might be
360 decreasing with frequency simply because higher frequencies entail shorter cycles. Indeed,
361 when we corrected for this by dividing cycle-wise spike count by cycle length, and thereby
362 calculating firing rate, we found it to correlate positively with frequency (Figure 7D, second pair
363 of bars).

364 These analyses were performed on the MUA, which comprises the spiking activity of a variety of
365 cell types. It is possible that our findings on the MUA reflected the activity of FS interneurons
366 rather than excitatory neurons (Vinck et al., 2013a). To address this, we therefore sorted the
367 MUA into single units. We classified these single units into broad and narrow-waveform units,
368 which correspond to putative pyramidal cells and putative interneurons, respectively (Mitchell et
369 al., 2007; Vinck et al., 2013a). We then repeated the previous analyses on these putative cell
370 classes. We observed that both cell types exhibited a similar behavior to the MUA, i.e. their
371 firing rates were positively correlated with frequency (Figure 7D, three rightmost pairs of bars).
372 Thus, the relationship between unit firing and gamma cycle duration was opposite to the
373 prediction by the abovementioned model of E-I balance: In awake macaque V1, neuronal firing
374 rates were lower in longer gamma cycles.

375 We found that longer gamma cycles had higher amplitudes but were accompanied by lower
376 firing rates. At first sight, this appears puzzling, considering that one would expect high-
377 amplitude cycles to reflect high firing rates. One possible explanation is that unit activity was
378 more synchronized during longer gamma cycles. To investigate this, we computed spike-LFP
379 phase-locking for each MUA, separately for gamma cycles of different durations. Phase-locking
380 was quantified by the pairwise phase consistency (PPC) (Vinck et al., 2010b), which removes
381 potential biases due to spike count or spike rate. We found that spike-LFP phase-locking was
382 negatively correlated with frequency (Figure 8C, Figure 8D third pair of bars). Thus, in macaque
383 V1, longer gamma cycles exhibited neuronal spiking activity with lower firing rates, yet more
384 precise phase locking.

Spyropoulos et al., Gamma-cycle amplitude versus duration in macaque visual cortex

385   If gamma cycles with longer duration were accompanied by higher phase-locking, this entails
386   that firing rates showed a stronger modulation as a function of gamma phase. Thus, in longer
387   gamma cycles, firing rates might have been overall lower, but showing a stronger transient
388   peak. In fact, Atallah and Scanziani reported that in rodent CA3, long gamma cycles were
389   accompanied by strong, transient activation peaks. To directly examine how firing rates
390   depended on gamma phase, we divided each gamma cycle into eight non-overlapping phase
391   bins. We then computed the mean MUA firing rates for these different phase bins, separately for
392   gamma cycles of different durations. Comparing longer with shorter gamma cycles, we found
393   that in longer gamma cycles, firing rates were particularly strongly decreased at the non-
394   preferred gamma phase, but only weakly decreased at the preferred gamma-phase (Figure 8).
395   Note that this amounts to a greater depth of firing-rate modulation for longer gamma cycles,
396   which is consistent with the positive correlation between spike-LFP phase-locking and gamma
397   cycle duration (Figures 7C and 7D). Thus, in longer gamma cycles, synchrony was overall
398   enhanced, which was primarily accounted for by a decrease in firing at the non-preferred
399   gamma phase, but not by an increase in firing at the preferred gamma-phase.

DISCUSSION

Summary

402   Gamma oscillations likely play a critical role in cortical communication. Key parameters of the
403   gamma rhythm are its amplitude and its frequency. Amplitude and frequency of gamma
404   oscillations fluctuate considerably over time, which may have important consequences for the
405   way in which gamma subserves communication. It is unclear how spontaneous fluctuations in
406   gamma amplitude and frequency are related to one another, and to the changes in firing activity
407   in the local circuit. We addressed this question by recording local field potentials (LFPs) and
408   spiking activity from primary visual cortex of awake macaques. We developed a method to
409   detect the amplitude and duration of individual gamma cycles on broadband LFPs. We found
410   that in macaque V1, across gamma cycles (or half cycles), there is a positive correlation
411   between the cycles' amplitudes and durations. This is specific to amplitudes and durations taken
412   from the same cycles (or half cycles), and it is strongly diminished or absent if amplitudes and
413   durations are taken from neighboring cycles (or half cycles). This finding was not due to several
414   factors that can influence both amplitude and frequency, like the time after stimulus onset or
415   microsaccades.

416   We also found that the instantaneous amplitude and duration of individual gamma cycles have a
417   complex relationship with the power spectrum: The distribution of durations of gamma cycles is
418   aligned to the power spectral peak, whereas the distribution of amplitudes is skewed towards
419   lower frequencies. This indicates that the power spectrum in the gamma range fails to
420   accurately capture the distribution of amplitudes for a given gamma frequency, and, instead,
421   better reflects the distribution of gamma-cycle durations.

422   Next, we examined how neuronal spiking varies as a function of gamma-cycle duration. We
423   observed that the firing rates of single units and multi-unit activity (in spikes/s) are negatively

11

424 correlated with the duration of gamma cycles, whereas the strength of spike-LFP phase locking
425 is positively correlated with gamma-cycle duration. Finally, we revealed that these patterns can
426 be explained by the fact that the depth of firing rate modulation by gamma phase increases with
427 gamma cycle duration.

428 In summary, these results show that, in macaque V1, shorter gamma cycles have lower
429 amplitudes and synchrony yet higher firing rates, whereas longer gamma cycles have higher
430 amplitudes and synchrony yet lower firing rates. This suggests that long gamma cycles are
431 driven by a strong rhythmic inhibitory current that prolongs the cycle and leads to weaker overall
432 firing.

Comparison with previous work

434 A previous study has addressed the correlation between instantaneous amplitude and
435 frequency of gamma in the CA3 field of the rat hippocampus under several different conditions
436 (awake freely moving, anesthetized, in vitro) (Atallah and Scanziani, 2009). This study reported
437 a strong positive correlation between the amplitude of each gamma cycle and its duration. We
438 show here that these positive correlations can arise spuriously due to the employed analytical
439 approach, mostly through the detection of noisy fluctuations in the signal. Indeed, we find
440 correlations similar to (Atallah and Scanziani, 2009) in signals where a strong gamma rhythm is
441 absent, namely in the baseline period of our data and in synthetic $1/f^n$ noise. This likely also
442 applies to the correlation between gamma-cycle durations in the LFP and gamma-cycle
443 amplitudes in intracellular IPSC measurements (Figure 5F of (Atallah and Scanziani, 2009)),
444 because LFP and IPSC from neighboring sites are highly correlated (Haider et al., 2016). In
445 general, the detection of instantaneous amplitude and frequency is difficult, because of the
446 presence of non-stationarities in the analyzed signal, and filter-generated smearing between
447 adjacent data points in the time domain. For this reason, we implemented an algorithm for the
448 detection of gamma-oscillatory epochs, i.e. periods in the LFP which are dominated by gamma
449 oscillations. The correlations calculated for these periods remained positive, but were weaker
450 compared to (Atallah and Scanziani, 2009). This difference in magnitude between our findings
451 and (Atallah and Scanziani, 2009) is due to a variety of factors. A major factor is that, in our
452 data, gamma cycle amplitude and duration do not co-vary monotonically, but rather exhibit an
453 inverted U-curve relationship (Figure 6).

454 Another major difference between our results and (Atallah and Scanziani, 2009) is in the
455 instantaneous relationship of firing rates with gamma cycle amplitude and duration. In (Atallah
456 and Scanziani, 2009), multi-unit activity (MUA) in rodent CA3 was shown to be concentrated in
457 the descending phase of the gamma-filtered LFP and to decrease as a function of the duration
458 of the gamma cycle. By contrast, we found in awake macaque V1 that spiking activity is
459 negatively correlated with gamma cycle duration. We observed the same pattern when we
460 sorted the MUA into putative pyramidal cells and putative interneurons. By contrast, gamma-
461 cycle duration was positively correlated with the strength of MUA-LFP phase locking: longer
462 gamma cycles contained spikes that were more strongly phase locked. A plausible
463 interpretation of these results is that, in macaque V1, longer gamma cycles involve the relatively

12

Spyropoulos et al., Gamma-cycle amplitude versus duration in macaque visual cortex

synchronous recruitment of excitatory cells and, consequently, the relatively synchronous engagement of inhibitory interneurons, leading to the relative increase of the amplitude of gamma. On the other hand, during shorter gamma cycles, excitatory cells fire more often but also more asynchronously. This is likely accompanied by the more frequent but also more asynchronous firing of inhibitory cells. As a consequence, the network excitation and inhibition cancel each other out, resulting in the relative decrease of the amplitude of gamma oscillations. This conclusion is, indeed, supported by our finding that the modulation depth of MUA during the gamma cycle increases with the duration of the latter.

Mechanisms and consequences

Cortical gamma oscillations *in vivo* are thought to be typically generated by a PING mechanism, which entails an E-I balance (Börgers and Kopell, 2003; Csicsvari et al., 2003; Hasenstaub et al., 2005; Salkoff et al., 2015; Tiesinga et al., 2001; Vinck et al., 2013a; Vinck et al., 2013b). The correlation between gamma-cycle amplitude and duration requires variability in those two parameters, and this variability could originate in the excitatory or the inhibitory component, or both. Atallah and Scanziani suggest that variability stems primarily from the excitatory component: Stronger bouts of excitation lead to stronger bouts of inhibition, which in turn lead to longer network silencing and thus longer gamma-cycle duration. The predictions of this model are consistent with the reported experimental results of Atallah and Scanziani in the hippocampal system. In our analysis of awake macaque V1 gamma, the predictions hold partially: We do find longer gamma cycles to be of higher amplitude; however, we also find them to show lower firing rates. In the visual system, the excitatory component can actually be manipulated experimentally, by changing the contrast of the visual stimulus. When contrast is increased, and thereby excitatory drive is enhanced, this leads (for most contrast values) to gamma of higher amplitude, yet also of higher frequency (Henrie and Shapley, 2005; Jia et al., 2013b; Ray and Maunsell, 2010; Roberts et al., 2013). These considerations suggest that the general PING mechanism of gamma generation is likely implemented in hippocampus and visual cortex in quite distinct circuit architectures, with important consequences for the relative roles of excitation versus inhibition. Specifically, in visual cortex, gamma is very strongly influenced by contextual mechanisms, which involve the synchronization among distributed columns and which are most likely exerted through inhibition (Vinck and Bosman, 2016). For example, large gratings or large uniform color surfaces lead to strong enhancement of gamma and strong inhibition of firing rates (Gieselmann and Thiele, 2008; Jia et al., 2013b; Peter et al., 2019). Thus, the dominant driver of the observed correlation in visual cortex might be the variability in the inhibitory component: Stronger bouts of inhibition lead to gamma cycles of larger amplitude and longer duration, and also to lower firing rates with stronger gamma-phase locking of the spikes. Each of these predictions is consistent with our results.

Note that the LFP primarily reflects postsynaptic currents in the dendrites of pyramidal neurons. These dendrites have biophysical properties that lead to a low-pass filtering of the postsynaptic currents (Branco and Häusser, 2011). This low-pass filtering likely interacts with the resonant (essentially band-pass) properties of the PING circuits. External drive to the PING circuit

Spyropoulos et al., Gamma-cycle amplitude versus duration in macaque visual cortex

504 generates gamma, and the low-pass characteristic of the involved pyramidal cells attenuates
505 the amplitudes of faster gamma cycles. This might contribute to our observation that the
506 amplitudes of relatively long gamma cycles are relatively large.

507 We found systematic relationships between the instantaneous gamma-cycle duration on the one
508 hand, and instantaneous amplitude and spiking activity on the other hand. These relationships
509 could have important consequences for the generation of long-range gamma-synchronization.
510 Granger-causality analyses suggest that a gamma rhythm in primary visual cortex can entrain
511 gamma in higher visual areas (Bastos et al., 2015; Bosman et al., 2012; Roberts et al., 2013).
512 Furthermore, fluctuations in gamma frequency, either due to varying contrast or occurring
513 spontaneously, are matched between V1 and V2 (Roberts et al., 2013). Strong, synchronous
514 bouts of excitation in a lower area (e.g. V1) could induce a long gamma cycle both in the lower
515 and in the higher area, due to strong, subsequent inhibition that is triggered in both areas. This
516 could facilitate the emergence of gamma-coherence between the lower and higher visual area.

517 In natural vision, it is common that different stimuli activate multiple groups of neurons in
518 primary visual cortex that compete for impact onto higher visual areas. Attention biases this
519 competition such that the higher area is selectively receptive to the inputs of one of these
520 neuronal groups (attentional target), and ignores the inputs of the other populations (distractors)
521 (Bosman et al., 2012; Desimone and Duncan, 1995; Fries, 2015; Grothe et al., 2012; Reynolds
522 et al., 1999). There is evidence that selective communication between areas is mediated by
523 selective gamma synchronization (Bosman et al., 2012; Fries, 2015; Gregoriou et al., 2009;
524 Grothe et al., 2012). When multiple input populations converge onto a single post-synaptic
525 target, selective gamma synchronization can lead to selective information transmission (Akam
526 and Kullmann, 2012; Börgers et al., 2008). The extent to which information can be selectively
527 transmitted is affected by whether the competing gamma rhythms have different gamma
528 phases, different gamma-peak frequencies, or show fluctuations in their gamma-peak frequency
529 (Akam and Kullmann, 2012; Börgers et al., 2008; Lowet et al., 2017). Yet, the consequences of
530 specific relationships between gamma frequency and gamma amplitude or local spike
531 synchrony for inter-areal transmission remain to be explored. Our respective results may
532 therefore have important consequences for the mechanisms underlying selective inter-areal
533 gamma-synchronization, and should be implemented in future computational models.

ACKNOWLEDGEMENTS

Spyropoulos et al., Gamma-cycle amplitude versus duration in macaque visual cortex

AUTHOR CONTRIBUTIONS

Conceptualization, G.S., M.V., and P.F.; Methodology, G.S., M.V., and P.F.; Software, G.S., J.R.D., and M.V.; Formal Analysis, G.S., J.R.D., I.O., M.V., and P.F.; Investigation, G.S., J.R.D., M.L.S., C.A.B., B.L., A.P., J.K.-L., R.R., S.N., W.S., and P.F.; Writing – Original Draft, G.S., M.V., and P.F.; Writing – Review & Editing, all authors; Supervision, M.V. and P.F.; Funding Acquisition, W.S., M.V., and P.F..

COMPETING FINANCIAL INTERESTS

The authors declare no competing financial interests.

Spyropoulos et al., Gamma-cycle amplitude versus duration in macaque visual cortex

550 # STAR ★ METHODS

551 ## KEY RESOURCES TABLE

REAGENT or RESOURCE	SOURCE	IDENTIFIER
Experimental Models: Organisms/Strains		
Macaque monkeys	German Primate Center	N/A
Software and Algorithms		
Stimulus control: NIMH CORTEX software ARCADE Custom LabView code	NIMH N/A National Instruments	dally.nimh.nih.gov/index.html https://gitlab.com/esi-neuroscience/arcade https://www.ni.com/
MATLAB 2016b	MathWorks Inc.	www.mathworks.com
FieldTrip Toolbox	(Oostenveld et al., 2011)	www.fieldtriptoolbox.org
Other		
ECoG Grid	(Rubehn et al., 2009)	N/A
CerePort ("Utah") array	Blackrock Microsystems	https://www.blackrockmicro.com
SC32-1 array	Gray Matter Research	https://www.graymatter-research.com/
Hydraulic Microdrives	Narishige Scientific Instrument Laboratory	https://www.narishige.co.jp/english/
PZ2 pre-amplifier	Tucker Davis Technologies	https://www.tdt.com/
RZ2 amplifier	Tucker Davis Technologies	https://www.tdt.com/
RS4 data streamer	Tucker Davis Technologies	https://www.tdt.com/
Digital Lynx system	Neuralynx	www.neuralynx.com
Plexon pre-amplifier	Plexon	www.plexon.com
Headstage amplifier	Plexon	www.plexon.com
E-series acquisition board	National Instruments	https://www.ni.com/
Eyelink 1000	SR Research Ltd.	https://www.sr-research.com/
Scleral search coil	Crist Instruments	http://www.cristinstrument.com/
ET-49B system	Thomas Recording	www.thomasrecording.com

552 ## CONTACT FOR REAGENT AND RESOURCE SHARING

553 Further information and requests for resources should be directed to and will be fulfilled by the
554 Lead Contact, Pascal Fries (pascal.fries@esi-frankfurt.de).

555 ## EXPERIMENTAL MODEL AND SUBJECT DETAILS

556 We analyzed data from a total of 6 adult macaque monkeys (*macaca mulatta*), referred to as
557 monkey H, I, J, L, P and T. Monkeys I and L are/were female, the others male. The experiments
558 were approved by the responsible regional or local authority, which was the
559 Regierungspräsidium Darmstadt, Germany, for monkeys H, I, J, L and T, and the ethics
560 committee of the Radboud University, Nijmegen, Netherlands, for monkey P. Parts of the data
561 have been used in other publications (Lima et al., 2010; Onorato et al., 2019; Vinck et al.,
562 2010a; Womelsdorf et al., 2012).

Spyropoulos et al., Gamma-cycle amplitude versus duration in macaque visual cortex

METHOD DETAILS:

Recordings

We used different recording procedures and stimulus paradigms for the different monkeys, and will describe these separately for the different monkeys.

Task

All monkeys performed a passive fixation task. The specific details of the task performed by monkeys I and P were as follows: Monkeys initiated a trial by depressing a lever (monkey I) or touching a bar (monkey P), which triggered the appearance of a fixation point, and then brought their gaze into a fixation window around the fixation point. Monkeys were required to fixate on the fixation point, which was centered on a gray background, after which a stimulus was presented. If they kept their gaze within the fixation window as long as the stimulus was presented, they were given a juice reward after the release of the lever/bar following stimulus offset. Monkeys H, J, L and T performed a similar task, with the initiation/termination of the trial being solely dependent on the acquisition/release of fixation (i.e. not dependent on pressing a lever or touching a bar). Further details of this version of the task are described in (Peter et al., 2019) for monkey H, and in (Lima et al., 2010) for monkeys J and L. For all monkeys, fixation windows ranged between 0.5 and 1.2 degrees radius.

Recordings (electrodes, reference)

For monkey H, recordings were done with CerePort ("Utah") arrays (64 micro-electrodes; inter-electrode distance 400 µm, tip radius 3-5 µm, impedances 70-800 kΩ, half of them with a length of 1 mm and half with a length of 0.6 mm, Blackrock Microsystems). A reference wire was inserted under the dura toward parietal cortex. Further details are reported in (Peter et al., 2019). For monkey I, a semi-chronic microelectrode array micro-drive was implanted over area V1 of the left hemisphere (SC32-1 drive from Gray Matter Research; 32 independently movable glass insulated tungsten electrodes with an impedance range of 0.5-2 MΩ and an inter-electrode distance of 1.5 mm, electrodes from Alpha Omega). We used the micro-drive chamber as the recording reference. For monkeys J and L, recordings were performed with 2 to 10 microelectrodes, made of quartz-insulated, tungsten-platinum material (diameter: 80 µm; impedances between 0.3 and 1MΩ; wire from Thomas Recording). These were inserted independently into the cortex via transdural guide tubes (diameter: 300µm; Ehrhardt Söhne), which were assembled in a customized recording device (designed by S.N.). This device consisted of 5 precision hydraulic micro-drives mounted on an X-Y stage (MO-95, Narishige Scientific Instrument Laboratory, Japan), which was secured on the recording chamber by means of a screw mount adapter. Inter-electrode distance ranged between 1 and 3 mm. We used the micro-drive chamber as the recording reference. Further details are reported in (Lima et al., 2010). For monkey P, we recorded neuronal activity with a micro-machined 252-channel electrocorticogram (ECoG) electrode array implanted subdurally on the left hemisphere (Bosman et al., 2012; Lewis et al., 2016; Rubehn et al., 2009). We used a silver ball implanted over occipital cortex of the right hemisphere as the recording reference. For monkey T, we

Spyropoulos et al., Gamma-cycle amplitude versus duration in macaque visual cortex

602 recorded neuronal activity with a micro-machined 252-channel ECoG electrode array implanted
603 subdurally over areas V1 and V4 of the left hemisphere (252 electrodes; inter-electrode distance
604 1400 μm; electrode diameter 400 μm, IMTEK & BCF, University of Freiburg) (Rubehn et al.,
605 2009). We used an electrode adjacent to the lunate sulcus as a recording reference for the
606 section of the array covering area V1.

Recordings (acquisition, filtering)

608 For monkeys H, I and T, we acquired data with Tucker Davis Technologies (TDT) systems. Data
609 were filtered between 0.35 and 7500 Hz (3 dB filter cutoffs) and digitized at 24,414.0625 Hz
610 (TDT PZ2 preamplifier). For monkeys J and L, we obtained spiking activity and the LFP by
611 amplifying 1000 times and band-pass filtering (0.7-6.0 kHz for MUA; 0.7-170 Hz for LFP) with a
612 customized 32-channel Plexon pre-amplifier connected to an HST16o25 headstage (Plexon
613 Inc., USA). Additional 103-fold signal amplification was performed by onboard amplifiers (E-
614 series acquisition boards, National Instruments, USA). For monkey P, we acquired data with a
615 Neuralynx system. Data were amplified 20 times, high-pass filtered at 0.159 Hz, low-pass
616 filtered at 8 kHz, and digitized at 32 kHz by a Neuralynx Digital Lynx system.

Receptive field mapping/Eccentricities

618 Receptive fields (RFs) were mapped with either bar stimuli ((Lima et al., 2010; Peter et al.,
619 2019); monkeys H, I, J, L), patches of moving gratings ((Bosman et al., 2012); monkey P) or
620 red dots (monkey T). The signal used for RF mapping was multi-unit activity (MUA) for
621 monkeys H, I, J, L, and the LFP gamma power for monkeys P and T. For monkeys J and L, we
622 recorded neuronal activity from the opercular region of area V1, leading to RF-center
623 eccentricities of 2-3 deg, and occasionally from the superior bank of the calcarine sulcus,
624 leading to RF-center eccentricities of 10-13 deg. For monkey H, RF-center eccentricities ranged
625 between 5.2 and 7.1 deg (median RF-center eccentricity 6.2 deg). For monkey I, RF-center
626 eccentricities ranged between 2.6 and 6.7 deg (median RF-center eccentricity 4.5 deg). For
627 monkey P, RF-center eccentricities ranged between 3 and 5.7 deg (median RF-center
628 eccentricity 4.6 deg). For monkey T, RF-center eccentricities ranged between 3.1 and 7.1 deg
629 (median RF-center eccentricity 3.8 deg).

Eye position monitoring

631 For monkeys H, I and T, eye movements and pupil size were recorded at 1000 Hz using an
632 Eyelink 1000 system (SR Research Ltd.) with infrared illumination. For monkeys J and L, we
633 monitored the eye position with a scleral search coil system (DNI, Crist Instruments, USA;
634 sampling rate of 500 Hz). For monkey P we monitored eye position with an infrared camera
635 system (Thomas Recording ET-49B system) at a sampling rate of 230 Hz. We used a
636 standardized fixation task in order to calibrate eye signals before each recording session.

Behavioral control and stimulus presentation

638 Stimulus presentation and behavioral control was implemented as follows: The software toolbox
639 ARCADE ((Dowdall et al., 2018) https://gitlab.com/esi-neuroscience/arcade) was used for

Spyropoulos et al., Gamma-cycle amplitude versus duration in macaque visual cortex

640   monkeys H, I and T; Custom LabVIEW code (Lab-VIEW, National Instruments, USA) was used
641   for monkeys J and L; The software toolbox CORTEX (dally.nimh.nih.gov/index.html) was used
642   for monkey P.

643   Monkeys H and I were presented with full-screen uniform color surfaces. Surface color varied
644   across trials according to a pseudo-random sequence. For our analyses, we used the hue that
645   elicited the strongest gamma oscillations (monkey H RGB: 149 99 0; monkey I RGB: 255 0 0).
646   In a separate session, monkey I was also repeatedly presented with a full-screen drifting
647   square-wave red-and-green grating of a fixed initial phase and drift-direction (RGB for red 255 0
648   0 and green 0 255 0; spatial frequency: 1.5 cycles/degree; temporal frequency 2 Hz). Monkeys
649   J and L were presented with large drifting square-wave black-and-white gratings (spatial
650   frequencies: 1.25-2 cycles/degree; temporal frequencies: 1.4-2Hz) and plaid stimuli. Only the
651   gratings were used for our analyses. The gratings had a diameter of 8 degrees of visual angle
652   and were positioned at the average of the RF centers of the recorded MUA. In each trial, the
653   direction of the grating drift was randomly chosen from 16 directions (in steps of 22.5 degrees).
654   Monkey P was repeatedly presented with a full-screen drifting square-wave black-and-white
655   grating of a fixed initial phase and drift-direction (spatial frequency: ~1 cycle/degree; temporal
656   frequency ~1Hz). Monkey T was presented with full-screen uniform color surfaces, with the
657   color changing across trials according to a pseudo-random sequence. For our analyses, we
658   used two hues that elicited the strongest gamma oscillations (RGB: 255 0 0 and 0 0 255). In
659   separate sessions, monkey T was also presented with full-screen drifting square-wave colored
660   gratings of pseudo-random initial phases and drift-directions. For our analyses, we used the
661   gratings that elicited the strongest gamma oscillations (red-green RGB: 255 0 0 and 0 255 0 and
662   blue-yellow RGB: 0 0 255 and 255 255 0; spatial frequency: 1.5 cycles/degree; temporal
663   frequency 2 Hz). For monkeys H, I and T, stimuli were presented on 120 Hz LCD monitors
664   (Wang and Nikolić, 2011), without gamma correction. For monkeys J, L and P, stimuli were
665   presented on CRT monitors (100-120 Hz), after gamma correction.

Data analysis

667   All analyses were done in MATLAB (The MathWorks) using custom scripts and the FieldTrip
668   toolbox (www.fieldtriptoolbox.org (Oostenveld et al., 2011)). The analyses were done only on
669   correct trials. In monkeys P and T, we selected the 25% electrodes/sites over area V1 with the
670   strongest visually induced gamma band activity, because the grids covered a relatively large
671   region of retinotopic space and contained electrodes that were poorly driven by the visual
672   stimulus. In monkeys H, I, J and L, we analyzed all visually driven electrodes. In all monkeys
673   except for monkey T, we analyzed LFP signals that were recorded relative to the common
674   reference signal (described above). For monkey T, we calculated local bipolar derivatives
675   between LFPs from immediately neighboring electrodes. i.e., differences (sample-by-sample in
676   the time domain), similar to previous studies (Bastos et al., 2015; Bosman et al., 2012). This
677   was done because the global references in monkey T were positioned over V1 and V4 in the
678   same hemisphere.

Spyropoulos et al., Gamma-cycle amplitude versus duration in macaque visual cortex

Preprocessing

For monkeys H, I and T, LFPs were obtained from the broadband signal after low-pass filtering (sixth order Butterworth filter with a corner frequency of 500 Hz), high-pass filtering (third order Butterworth filter with a corner frequency of 2 Hz for monkey T and 4 Hz for monkeys H and I) and down-sampling to 2034.51 Hz. For monkeys J and L, LFPs were filtered between 0.7-170Hz (hardware-filter, described above) and down-sampled to 1 kHz. For monkey P, we obtained LFP signals by low-pass filtering at 200 Hz and down-sampling to 1 kHz. In addition, for monkey P, we removed powerline artifacts at 50 Hz and its harmonics with a digital notch filter.

Segmenting Data into Epochs, and Calculation of Power and TFR

To estimate the LFP power spectra in the stimulus and baseline periods (Figures 1B, 1C, 1G and1H, Figure 6, Figures 7A-7C), we used the following procedure: Power spectra were estimated separately for the pre-stimulus period and the stimulation period. The pre-stimulus period was the time between fixation onset and stimulus onset. During the pre-stimulus period, monkeys fixated on a central dot on a gray screen, and there was no other stimulus presented. For monkeys H, I, P and T, the pre-stimulus and stimulation periods were of variable length across trials. We kept data corresponding to the pre-stimulus and stimulation period with the minimum length (monkey H: baseline 0.3s / stimulation 1.5s; monkey I: baseline 0.5s / stimulation 2s; monkey P: baseline 0.3s / stimulation 2.3s; monkey T: baseline 1.1s / stimulation with full-screen gratings 2.8s / stimulation with full-screen uniform color surfaces 3.2s). For monkeys J and L, the pre-stimulus and grating-stimulation periods had a stable duration across trials within a session but their duration varied between sessions. All of the available pre-stimulus and grating data were analyzed for those monkeys (baseline 0.8-1s / stimulation 2-2.4s). The power spectral analysis was based on epochs of fixed lengths. Therefore, the described task periods were cut into non-overlapping epochs. We aimed at excluding data soon after stimulus onset ("event") to minimize the influence of the stimulus-onset related event-related potential on our analyses. Therefore, periods were cut into non-overlapping epochs, starting from the end of the period and stopping before an epoch would have included data approximately 0.5 s after those events. For Figures 1B, 1C, 1G and 1H, the estimation of power spectra was based on epochs of 0.5 s length; for Figures 6 and S2B, power spectra were based on epochs of 0.25 s. Data epochs were Hann tapered, to achieve a fundamental spectral resolution (Rayleigh frequency) of 2 Hz (4 Hz for figures 6 and S2B), and then Fourier transformed. For the time-frequency analysis of power, we used window lengths of ±2.5 cycles per frequency which were slid over the available data in steps of 1 ms. Power during the stimulation period was normalized to the pre-stimulus baseline period, separately for each channel, in the following manner: Power per frequency and per trial was calculated as described above. Power calculated for the pre-stimulus baseline period was then averaged across trials. Finally, trial-wise normalized power was calculated for the stimulation period by subtracting the average pre-stimulus spectrum and then dividing by it.

Spyropoulos et al., Gamma-cycle amplitude versus duration in macaque visual cortex

Spike sorting

718 Single units were isolated through semi-automated spike sorting (Onorato et al., 2019). First, we
719 performed semi-automatic clustering with the KlustaKwik 3.0 software. The energy of the spike
720 waveform and the energy of its first derivative were used as features in this procedure. A
721 candidate single unit was accepted if the corresponding cluster was clearly separable from the
722 noise clusters, and if the inter-spike-interval distribution had a clear refractory-period. This was
723 done manually with the M-Clust software. In addition, we used the isolation distance (ID;
724 (Schmitzer-Torbert et al., 2005)) as a measure of cluster separation. The ID of a candidate
725 single unit had to exceed 20 in order for it to be included in our analyses. The median ID was
726 25.05. This procedure led to the isolation of 100 single units. For each isolated single unit, we
727 computed the peak-to-trough duration of the average AP waveform. Single units with long
728 (>0.235ms) and short (<0.235ms) peak-to-trough durations were named "broad-waveform"
729 (BW) and "narrow-waveform" (NW) neurons, respectively. Broad-waveform neurons
730 corresponded to 29% of the single unit population.

Initial estimation of gamma-cycle amplitude and duration (cf. Atallah & Scanziani)

733 For our initial analyses of individual gamma cycles, we implemented the algorithm as described
734 by Atallah and Scanziani (2009) for data from awake freely-moving rats. In short, we first low-
735 pass filtered the LFP by using a 40 ms moving average filter and then subtracted this filtered
736 signal from the original time series (Experimental Procedures and Supplemental Experimental
737 Procedures of Atallah and Scanziani, and their personal communication with us), which
738 effectively corresponds to a high-pass filter with a corner frequency at approximately 20 Hz. The
739 resulting signal was further band-pass filtered in the range of 5-100 Hz with a 3rd order, two-way
740 Butterworth filter. Gamma-cycle peaks and troughs were then defined as local maxima and
741 minima, respectively. Furthermore, gamma-cycle amplitudes were defined as the difference
742 between the voltage of a given peak and its subsequent trough. Similarly, gamma-cycle
743 durations were defined as the interval between a given peak and it subsequent peak. This
744 analysis was done in segments of the filtered signal which displayed high power in the individual
745 gamma frequency range of each dataset (peak gamma frequency±20 Hz). These segments
746 were extracted in the following way: A time-power representation of each trial was calculated
747 with 5 discrete prolate slepian sequences and windows of 100 ms which were slid over the
748 available data in steps of 25 ms. Gamma episodes were defined as segments of the resulting
749 time-series which lasted for more than 100 ms and had power that exceeded a threshold. This
750 threshold was calculated separately for each trial as the difference between the mean of the
751 time-power representation and its standard deviation.

Generation of colored noise

753 In Figure 2G, we analyzed the correlations obtained with the Atallah-Scanziani method for
754 colored noise. We generated noise with power spectra following a $1/f^n$ function, where f denotes
755 frequency and n assumes 11 equally spaced values between, and including, 0 (corresponding
756 to white noise) and 2 (corresponding to Brownian noise). This was done in the following
757 manner: (i) 1000 white noise traces containing 10^6 samples were generated for each n. (ii) Each

21

Spyropoulos et al., Gamma-cycle amplitude versus duration in macaque visual cortex

758 trace was Fourier transformed. (iii) The complex coefficients of the positive frequencies in the
759 resulting spectra were multiplied by the $1/f^n$ function. (iv) A synthetic spectrum was constructed
760 by concatenating the above complex coefficients with the conjugate of their flipped version. (v)
761 The resulting spectrum was inverse Fourier transformed to obtain time series.

Improved estimation of gamma-cycle amplitude and duration

763 We developed an improved method to extract gamma-cycle amplitude and frequency from the
764 LFP signals as follows:

765 1. We computed the Hilbert-transform of the broadband LFP signal to obtain the analytic signal
766 and derive the time-resolved phase from it. We used the broadband signal, because band-pass
767 filtering creates dependencies between voltage values across time points, and can transform
768 transient, non-oscillatory deflections into rhythmic events.

769 2. We detected gamma cycles as follows: First, we detected all the zero-crossings of the phase.
770 Such phase zero crossings occur in the neighborhood of peaks and troughs in the original LFP
771 signal. For each k-th zero-crossing, we examined whether the angular velocity of the phase was
772 positive for all time points between the k - 1-th to the k + 1-th zero-crossing (similar to (Muller et
773 al., 2014)). If this was not the case, then there was a negative "phase-slip" in which the
774 instantaneous frequency became negative, and the respective zero crossing plus/minus two
775 neighboring zero crossings were discarded. Negative instantaneous frequencies make the
776 interpretation of the instantaneous frequency and amplitude ambiguous, and are typically
777 accompanied by small peaks/troughs in the LFP signal. This violates our model of the gamma
778 oscillation as a signal with a positive frequency which fluctuates over time, $y(t) = A(t) * \cos$
779 $(\omega(t)*t + \varphi)$, where $A(t)$ and $\omega(t)$ are the instantaneous amplitude and frequency fluctuating
780 over time.

781 If there was no negative phase-slip, then we identified gamma peaks by first detecting negative-
782 to-positive zero crossings in the phase of the analytic signal. For each of these crossings, we
783 then identified the nearest local maximum in the LFP signal (Figure 3D). Likewise, gamma
784 troughs were identified by detecting positive-to-negative zero crossings and identifying nearby
785 local minima. Using the detected gamma peaks and troughs, we then determined the gamma-
786 cycle amplitude and duration. To obtain estimates of gamma-cycle amplitude and duration with
787 the maximum attainable temporal resolution, we divided each gamma cycle into "half-cycles":
788 The first half-cycle comprised the data segment from the trough to the peak, and the second
789 half-cycle from the peak to the trough. For each half-cycle, amplitude was defined as the
790 difference between the respective peak and trough, and duration was defined as the
791 corresponding time interval. For each detected half-cycle, we thus obtained an amplitude and
792 duration value. For comparison, we also determined amplitude and duration for full gamma
793 cycles. A gamma cycle comprised the data from one peak to the next peak. Amplitude was
794 defined as the voltage difference between the first peak and the trough. Duration was defined at
795 the time between the two peaks.

Spyropoulos et al., Gamma-cycle amplitude versus duration in macaque visual cortex

796 Note that for the analysis of the relationship between individual gamma cycles and spiking
797 activity, we used a band-pass filter (3rd order, two-pass Butterworth, with a pass-band of 40-90
798 Hz for monkey J and 25-55 Hz for monkey L). In this case, we used an additional criterion to
799 reject epochs of spurious oscillatory activity (Onorato et al., 2019): We ran the same cycle-
800 selection procedure on the pre-stimulus period, in which narrow-band gamma-band oscillations
801 are virtually absent. For the pre-stimulus period, we obtained the mean μ_{pre} and standard
802 deviation σ_{pre} of the distribution of amplitudes. These amplitudes were measured as the peak-to-
803 trough distance of the gamma cycle. A cycle in the stimulus period with amplitude A was only
804 selected if $(A - \mu_{pre})/\sigma_{pre} > 1{:}63$ (which is equivalent to a one-sided T-test at P < 0.05). We
805 filtered the LFP with the purpose of increasing the number of selected gamma epochs,
806 considering that the analysis of unit firing rates and spike-field phase-locking demands a
807 relatively large amount of data. Note that we have shown in Figure 7 that the distributions of
808 amplitude and frequency after band-pass filtering are comparable to the distributions obtained
809 without band-pass filtering. In addition, the potential issues related to filtering only apply to the
810 calculation of correlations of amplitude and duration and not to the calculation of the correlation
811 of spiking strength and gamma frequency. This is due to the fact that filtering may generate
812 artificial correlations between the amplitudes and durations of deflections of the same time
813 series (explained further in the results section). The filter used on the LFP is not used on the
814 spiking activity. Thus, artificial correlations between spiking and cycle-by-cycle frequency are
815 not likely.

816 Amplitude and frequency values were extracted from selected gamma epochs of a duration of at
817 least 2 full cycles.

Computation of time-resolved correlations between amplitude and frequency

819 In the case of our V1 recordings, we observed that gamma amplitude and cycle duration
820 progressively increased over time after the onset of a drifting grating stimulus. (Figures 1C-1D).
821 By contrast, after the onset of a uniform color surface, gamma amplitude and duration
822 progressively decreased and increased over time, respectively (Figures 1G-1H). These changes
823 with time after stimulus onset could contribute to the correlation values between gamma-cycle
824 amplitude and duration, if gamma amplitude and duration values are concatenated across all
825 trials and time points. This would conceal the relationship between gamma-cycle amplitude and
826 duration due to intrinsic variability, by introducing a positive or negative correlation bias for
827 drifting gratings and uniform color surfaces, respectively.

828 We avoided these effects by using the following method: We calculated correlations between
829 gamma-cycle amplitudes and durations across all trials, separately for each time point (at the
830 respective sampling rate) after stimulus onset, and subsequently averaged those correlation
831 values over time points and subsequently over recording sites. To enable this, we needed to
832 define gamma-cycle amplitudes and durations for each time point. Therefore, each time point
833 (relative to stimulus onset) was localized to the gamma half cycle (or full cycle), into which it fell,
834 and it was assigned the respective amplitude and duration of that half cycle (or full cycle). For
835 the calculation of correlations with one or multiple half-cycle (or full-cycle) lags, correlations

Spyropoulos et al., Gamma-cycle amplitude versus duration in macaque visual cortex

836 were calculated between amplitudes and durations shifted relative to each other by the
837 corresponding number of half-cycles (or full cycles).

838 In datasets containing more than one stimulus condition, correlation coefficients were calculated
839 separately for each condition and then averaged across conditions.

840 As mentioned in the results section, the correlation analysis used the Spearman correlation
841 coefficient. Like in (Atallah and Scanziani, 2009), we found results to be essentially identical for
842 Spearman and Pearson correlation, when using their method of determining gamma amplitude
843 and duration. For the rest of our analyses, we used exclusively the Spearman correlation
844 coefficient.

Statistical significance of correlations

846 The statistical significance of correlations between gamma-cycle amplitudes and durations was
847 assessed by means of a non-parametric randomization approach: The order of valid duration
848 values was randomly shuffled across trials, separately for each time-point. We then calculated
849 surrogate Spearman's correlation coefficients 1000 times as described above for each dataset.
850 Next, we performed a fit of a Gaussian distribution on the 1000 surrogate correlation
851 coefficients. Empirical correlations were deemed significant if they were 3 standard deviations
852 larger or smaller than the mean of the surrogate distribution. This procedure implements a non-
853 parametric version of a two-sided test with a p-value of ≈0.001.

854 To test if the mean correlation of gamma-cycle amplitudes and durations is significantly different
855 from zero across datasets, we applied a Student's t-test. In general, we prefer non-parametric
856 randomization tests over parametric tests (like the t-test). However, some analyses contained
857 only four or five datasets, which effectively precludes the application of non-parametric tests.
858 Where possible, we supplemented the t-test with a non-parametric statistical test (Figures 2C,
859 4A, 4B and S1A). Specifically, we calculated the mean correlation across datasets for each
860 possible combination of values that results after independently inverting or maintaining the sign
861 of each correlation value (i.e. a full permutation). This led to a surrogate distribution of mean
862 values to which the empirical mean was compared for statistical significance. Mean correlations
863 were deemed significant if they were larger (smaller) than the top (bottom) 2.5 percentile of this
864 surrogate distribution.

Regression analysis

866 We performed regression analyses separately for gamma-cycle amplitudes and durations with
867 the Matlab function *regress*. As explained in the results section, for each half-cycle, we
868 regressed the amplitude value of the ongoing half-cycle against the amplitude values of the
869 previous and next half-cycle, by using a least squares approach. We used the same procedure
870 for half-cycle duration values. This was done for each point after stimulus onset separately, and
871 by using all the amplitude and duration values across trials (for that time point). We then
872 calculated the regression residuals by subtracting each amplitude and duration regression
873 vector from the corresponding amplitude and duration values, separately for each timepoint.

24

Spyropoulos et al., Gamma-cycle amplitude versus duration in macaque visual cortex

874   These residual values measured the extent to which the amplitude or duration in the ongoing
875   half-cycle was greater or smaller than in the surrounding half-cycles, and thereby departed from
876   slower trends. We then computed the correlation between the regression residuals for amplitude
877   and duration, in the same way as described above.

878 **Micro-saccade detection**

879   We low-pass filtered vertical and horizontal eye position signals by replacing each value with the
880   average over itself ±15 ms. We then computed the first temporal derivative of the signals to
881   obtain the vertical and horizontal velocities. We combined those values to obtain the eye speed
882   irrespective of the direction of eye movement. Per trial, we determined the SD of eye speed,
883   and any deviation >4 SDs and lasting for at least 30 ms was deemed a saccadic eye
884   movement. Saccadic eye movements that remained within the fixation window were considered
885   to be MSs.

886 **AR**

887   In Figure S2, we computed our correlations for data generated through auto-regressive models
888   with a power spectrum similar to the recorded LFP data. An autoregressive (AR) model of
889   order n represents each value in a time-varying process as the linear sum of its n preceding
890   values (each weighted by a separate coefficient) and a stochastic term. This model can then be
891   used to generate a synthetic time series that has the same power spectrum as the original
892   process, but that is devoid of higher-order statistical properties such as slow temporal trends or
893   spectral cross-frequency dependencies. We modelled the LFP as an AR process of a relatively
894   high order (50 for monkeys J and P, whose analysis was based on a sampling rate of 1000 Hz,
895   and 100 for monkeys H, I, T, whose analysis was based on a sampling rate of 2034.51 Hz). We
896   did this by fitting a vector of AR coefficients and a noise variance term with the Matlab function
897   *arfit*, simultaneously to all the trials of a given stimulus condition and independently for each
898   recording site. For our analyses, we only used the period of the trial starting at 250 ms after
899   stimulus onset, thereby omitting stimulus onset-related transient activity. These AR models were
900   then used to generate surrogate time series.

901 **PPC**

902   For the calculation of spike-LFP PPC, the gamma phase of each spike within a gamma cycle
903   was defined as $t/T*2*\pi$, where t was the time of the spike relative to the start of the gamma
904   cycle, and T was the duration of the gamma cycle. This constitutes a linear phase interpolation.
905   This used the improved Hilbert-based definition of gamma half-cycles (cycles). The obtained
906   spike phases from separate trials were collected, and the average consistency of phases across
907   these pairs was estimated with the pairwise-phase-consistency metric (PPC) (Vinck et al., 2012;
908   Vinck et al., 2010b), and more specifically its PPC1 variant (Vinck et al., 2012). Any potential
909   bias due to differences in discharge rates is removed by the pairwise computation. Only
910   neurons that fired at least 50 spikes were considered, because phase-locking estimates can
911   have a high variance in cases of low spike counts. We were not able to perform this analysis for
912   single-unit activity, due to the lack of a sufficient number of detected single unit spikes.

Spyropoulos et al., Gamma-cycle amplitude versus duration in macaque visual cortex

Computation of the Cycle-Based-Spectrum (CBS) and rate-of-incidence of gamma-frequencies

For Figure 6, we computed the cycle-based-spectrum (CBS) and the rate-of-incidence of different gamma-frequencies as follows. Gamma half-cycle amplitude and duration values were extracted from the LFP through the use of the previously described improved detection algorithm. Values of gamma-half-cycle durations were converted into values of gamma-half-cycle frequency (frequency being the inverse of duration). This was done separately for each recording site and stimulus condition. Next, gamma half cycles were assigned to their corresponding frequency bin, and for each frequency bin, the average amplitude and the rate of incidence of that frequency were determined.

Note that the peak gamma-frequency varies across experimental subjects and stimulus conditions. In order to compute averages across stimulus conditions and monkeys, it is therefore necessary to align individual distributions to the power-spectral peak in the gamma-frequency-range, separately for each stimulus condition and dataset. We performed this alignment in the following way: The raw trial-wise power spectra were estimated separately for each stimulus condition as described above (see power), and from these spectra we determined the peak gamma-frequency. In addition, this was done for the baseline-corrected power spectra. The alignment of half-cycle amplitudes and frequency counts was then performed around the resulting frequency. Specifically, half-cycle amplitude and frequency count averages at ±20 Hz around the gamma peak were averaged across stimulus conditions and datasets. Note that we analyzed datasets with different sampling rates. This entailed that the range of detectable half-cycle frequencies (i.e. sampling rate/(2*duration)) varied across different datasets and, depending on the sampling rate, certain frequency bins were necessarily empty. In order to average across datasets with different sampling rates, we therefore performed a linear interpolation between normalized half-cycle amplitude values and frequency counts, which were adjacent to empty bins.

Spyropoulos et al., Gamma-cycle amplitude versus duration in macaque visual cortex

Legends

Fig. 1. Gamma dynamics in monkey V1 during visual stimulation. (A) Raw LFP trace from one representative recording site from area V1 in monkey T before and during the presentation of a full-screen drifting grating. (B and C) Raw power (B) and power change relative to baseline (C), averaged across all selected recording sites from V1 in monkey T. The green and black traces in (B) correspond to the pre-stimulus baseline period and stimulation period respectively. The error regions show 2 standard errors of the mean (S.E.M.) based on a bootstrap procedure across trials (1000 bootstraps). (D) Power change relative to baseline, as function of frequency and time relative to stimulus onset, averaged over all selected V1 recording sites in monkey T before and during the presentation of a full-screen drifting grating. Note the changes in gamma amplitude and frequency with time after stimulus onset. (E) Time course of gamma-half-cycle amplitude (blue) and duration (red), averaged over all selected V1 recording sites in monkey T during the presentation of a full-screen drifting grating. The error regions show ±2 SEM based on a bootstrap procedure. Only the stimulation period is shown, because only very few gamma cycles of very low amplitude were detected before stimulus onset. (F-J) Same as A-E, but for the presentation of a full-screen uniform color surface. (A, D, F, I) Dashed lines indicate stimulus onset.

Fig. 2. Estimation of correlation between gamma-cycle amplitude and duration can be influenced by noise. (A) Representative LFP trace filtered in the gamma range (20-100 Hz). Red dots indicate local maxima and minima. (B) Initial segment of the trace in (A) demonstrating the definition of gamma-cycle amplitude and gamma-cycle inter-event interval (IEI), which we refer to as duration. (C) For each dataset listed on the x-axis, the three bars show the correlation between gamma-cycle amplitudes and the durations of the same gamma cycle (center, red), the previous gamma cycle (left, white) and the next gamma cycle (right, white). On the right, this is shown for the average across all datasets. This was calculated for the period during the presentation of the visual stimulus. Amplitude and duration values were extracted as in (Atallah and Scanziani, 2009) for data from awake freely-moving rats. This includes the filtering illustrated in (A, B); note that the employed subtraction of a boxcar-smoothed signal amounts to a high-pass-filtering at 20 Hz (see Methods for details). For each individual dataset, a null distribution was produced by randomizing the order of duration values across trials, and the resulting means and 99.9% confidence intervals are shown as dots and vertical lines (all very close to the zero line). For the average across datasets, shown on the right, we performed a t-test and show the resulting confidence intervals as vertical lines on the observed mean. (D) Same as (C) but for the pre-stimulus baseline. (E) Example synthetic colored noise trace filtered in the gamma range (20-100 Hz). Red dots indicate local maxima and minima. (F) Power spectra of synthetic colored noise signals with a spectral shape of $1/f^n$, with n assuming values from 0 (dark blue) to 2 (bright yellow). (G) Correlation of the amplitude and duration of individual deflections in synthetic colored noise signals. Dots and vertical lines indicate means ±2 SEM produced by a bootstrap procedure (1000 bootstraps). The color conventions are the same as in (F).

Spyropoulos et al., Gamma-cycle amplitude versus duration in macaque visual cortex

979 **Fig. 3. Illustration of a method for the selection of gamma-oscillatory epochs.** (A) LFP
980 trace displayed in Figure 1A, with regions presented in red corresponding to gamma epochs
981 passing the criterion for stationarity. (B) Phase of the analytic signal based on the Hilbert
982 transform of the trace shown in A. (C) Angular velocity of A. Note periods of positive and
983 relatively stable angular velocity, corresponding to oscillatory gamma epochs in the original
984 LFP. (A-C) Dashed lines indicate stimulus onset. (D) Magnification of the designated section of
985 the LFP trace and its phase. Red dots indicate detected LFP peaks and troughs. Vertical
986 dashed lines designate negative-to-positive and positive-to-negative zero crossings of the
987 phase of the analytic signal, whereas horizontal dashed lines designate 0.

988 **Fig. 4. Gamma-half-cycle amplitudes and durations are positively correlated in gamma-**
989 **oscillatory epochs.** (A) For each dataset listed on the x-axis, the three bars show the
990 correlation between the amplitude of a gamma half cycle and the duration of the same gamma
991 half cycle (center, red), previous gamma half cycle (left, white) and next gamma half cycle (right,
992 white). On the right, this is shown for the average across all datasets. This was calculated for
993 each time-point across trials and averaged across time-points for gamma-oscillatory epochs.
994 The data used correspond to the period during the presentation of the visual stimulus. For each
995 individual dataset, a null distribution was produced by randomizing the order of duration values
996 across trials, and the resulting means and 99.9% confidence intervals are shown as dots and
997 vertical lines. For the average across datasets, shown on the right, we performed a t-test and
998 show the resulting confidence intervals as vertical lines on the observed mean. (B) Correlation
999 between the amplitude of a gamma half-cycle and the duration of gamma half-cycles before and
1000 after it for 3 different datasets. Note that in monkey I, this is limited to ±2 cycles, because the
1001 signal-to-noise ratio was lower, resulting in shorter gamma-oscillatory epochs. Importantly, all
1002 three example datasets show a central peak, despite the fact that they show different longer-
1003 term correlations, including a relatively broad peak in the middle trace and a relatively broad
1004 trough in the right trace. The gray lines and gray-shaded areas depict the means and
1005 99.9% confidence regions, after randomizing the order of duration values across trials.
1006 (C) Same as A, but showing the correlations between residuals of the regression across
1007 adjacent amplitude triplets and the residuals of the regression across adjacent duration triplets.

1008 **Fig 5. The effect of MSs on the correlation between gamma-half-cycle amplitudes and**
1009 **durations.** (A) Time-frequency power averaged over all selected V1 recording sites in monkey
1010 T during the presentation of a full-screen drifting grating, normalized by the pre-stimulus
1011 baseline. X-axis shows time relative to detected microsaccades (MSs). (B) Time-course of the
1012 gamma-half-cycle amplitude (blue) and duration (red) of the data depicted in A. Error regions
1013 show ±2 SEM based on a bootstrap over MSs. (C) Same as Figure 4C, but after the removal of
1014 250 ms epochs following the occurrence of MSs for all available datasets.

1015 **Fig 6. Cycle-based spectra of amplitudes and rates of incidence.** (A) The x-axis shows
1016 duration expressed as its inverse, namely frequency, and after aligning to the gamma peak in
1017 the raw power spectrum (black trace). The blue curve shows the gamma-half-cycle amplitudes
1018 as a function of their duration. The red curve shows the count of detected gamma half-cycles as

28

Spyropoulos et al., Gamma-cycle amplitude versus duration in macaque visual cortex

1019 a function of their duration. These analyses were based on the broadband signal from the last
1020 250 ms of stimulation (see Methods). Error regions show ±2 SEM based on a bootstrap
1021 procedure. (B) Same as A, but after aligning to the peak in the power change spectrum. (C)
1022 Same as A, and (D) same as B, but for gamma epochs detected on the filtered LFP.

Fig 7. The relationship between gamma-cycle duration and spiking. (A) The blue curve
depicts the average normalized multi-unit (MU) spike count in detected gamma cycles of
different durations, expressed on the x-axis as frequencies, for monkey J (left) and monkey L
(right). The black curve depicts raw power in the gamma range of the respective monkeys. Error
regions show ±2 SEM across units. (B) Same as A, but using the normalized MU firing rate. (C)
Same as A, but showing the normalized change in spike-LFP PPC. (D) Correlation between the
gamma-cycle duration, expressed as frequency, and several spiking metrics, separately for the
two monkeys (J and L). Vertical lines depict ±2 SEM across units.

Fig 8. The modulation of spiking activity by the phase of the gamma cycle. (A) The color
shows the modulation of the MU firing rate as a function of gamma-cycle duration (y-axis) and
the phase in the gamma cycle, at which spikes occurred (x-axis). (B) Difference in normalized
firing rate between short and long gamma cycles for the preferred (left bar) and non-preferred
phase in gamma cycles (right bar). Vertical lines depict ±2 SEM across units. Data from
monkey J and monkey L are shown in the left and right column, respectively.

Fig. S1. Gamma-full-cycle amplitudes and durations are positively correlated. (A) Same as
Figure 4A, but using full gamma cycles. (B) Same as Figure 4C, but using full gamma cycles.
(C) Same as Figure S2E, but using full gamma cycles. (D) Same as Figure 5C, but using full
gamma cycles.

**Fig. S2. Correlation of gamma-half-cycle amplitudes and durations in an AR model of the
visual stimulation period.** Panels (A-D) are based on signals generated by an autoregressive
(AR) model of the data used in Figures 1A-1D, stimulation period, averaged over all selected V1
sites. We refer to the synthetic LFP signal generated by the AR model as AR-based LFP.
(A) Representative AR-based LFP. Regions presented in red correspond to gamma epochs
passing the criterion for stationarity. (B) Average raw power of the measured (black) and the
AR-based LFP (green). (C) Time-frequency power of AR-based LFP. Note the expected
absence of temporal trends. (D) Time-course of gamma-half-cycle amplitude (blue) and duration
(red) of AR-based LFP. Error regions show ±2 SEM based on a bootstrap procedure. (E) Same
as Figure 4A, but for the AR-based LFP.

Spyropoulos et al., Gamma-cycle amplitude versus duration in macaque visual cortex

References

Akam, T.E., and Kullmann, D.M. (2012). Efficient "communication through coherence" requires oscillations structured to minimize interference between signals. PLoS computational biology 8, e1002760.

Atallah, B.V., and Scanziani, M. (2009). Instantaneous modulation of gamma oscillation frequency by balancing excitation with inhibition. Neuron 62, 566-577.

Bastos, A.M., Vezoli, J., Bosman, C.A., Schoffelen, J.M., Oostenveld, R., Dowdall, J.R., De Weerd, P., Kennedy, H., and Fries, P. (2015). Visual areas exert feedforward and feedback influences through distinct frequency channels. Neuron 85, 390-401.

Bichot, N.P., Rossi, A.F., and Desimone, R. (2005). Parallel and serial neural mechanisms for visual search in macaque area V4. Science 308, 529-534.

Bieri, K.W., Bobbitt, K.N., and Colgin, L.L. (2014). Slow and fast gamma rhythms coordinate different spatial coding modes in hippocampal place cells. Neuron 82, 670-681.

Börgers, C., Epstein, S., and Kopell, N.J. (2008). Gamma oscillations mediate stimulus competition and attentional selection in a cortical network model. Proceedings of the National Academy of Sciences of the United States of America 105, 18023-18028.

Börgers, C., and Kopell, N. (2003). Synchronization in networks of excitatory and inhibitory neurons with sparse, random connectivity. Neural computation 15, 509-538.

Bosman, C.A., Schoffelen, J.M., Brunet, N., Oostenveld, R., Bastos, A.M., Womelsdorf, T., Rubehn, B., Stieglitz, T., De Weerd, P., and Fries, P. (2012). Attentional stimulus selection through selective synchronization between monkey visual areas. Neuron 75, 875-888.

Bosman, C.A., Womelsdorf, T., Desimone, R., and Fries, P. (2009). A microsaccadic rhythm modulates gamma-band synchronization and behavior. The Journal of neuroscience : the official journal of the Society for Neuroscience 29, 9471-9480.

Bragin, A., Jandó, G., Nádasdy, Z., Hetke, J., Wise, K., and Buzsáki, G. (1995). Gamma (40-100 Hz) oscillation in the hippocampus of the behaving rat. The Journal of neuroscience : the official journal of the Society for Neuroscience 15, 47-60.

Branco, T., and Häusser, M. (2011). Synaptic integration gradients in single cortical pyramidal cell dendrites. Neuron 69, 885-892.

Brunet, N.M., Bosman, C.A., Vinck, M., Roberts, M., Oostenveld, R., Desimone, R., De Weerd, P., and Fries, P. (2014). Stimulus repetition modulates gamma-band synchronization in primate visual cortex. Proceedings of the National Academy of Sciences of the United States of America 111, 3626-3631.

Burns, S.P., Xing, D., and Shapley, R.M. (2011). Is gamma-band activity in the local field potential of V1 cortex a "clock" or filtered noise? The Journal of neuroscience : the official journal of the Society for Neuroscience 31, 9658-9664.

Spyropoulos et al., Gamma-cycle amplitude versus duration in macaque visual cortex

1088   Buschman, T.J., and Miller, E.K. (2007). Top-down versus bottom-up control of attention in the
1089   prefrontal and posterior parietal cortices. Science 315, 1860-1862.

1090   Buzsáki, G., and Wang, X.J. (2012). Mechanisms of gamma oscillations. Annual review of
1091   neuroscience 35, 203-225.

1092   Cardin, J.A., Carlén, M., Meletis, K., Knoblich, U., Zhang, F., Deisseroth, K., Tsai, L.H., and
1093   Moore, C.I. (2009). Driving fast-spiking cells induces gamma rhythm and controls sensory
1094   responses. Nature 459, 663-667.

1095   Colgin, L.L., Denninger, T., Fyhn, M., Hafting, T., Bonnevie, T., Jensen, O., Moser, M.B., and
1096   Moser, E.I. (2009). Frequency of gamma oscillations routes flow of information in the
1097   hippocampus. Nature 462, 353-357.

1098   Csicsvari, J., Jamieson, B., Wise, K.D., and Buzsáki, G. (2003). Mechanisms of gamma
1099   oscillations in the hippocampus of the behaving rat. Neuron 37, 311-322.

1100   Desimone, R., and Duncan, J. (1995). Neural mechanisms of selective visual attention. Annual
1101   review of neuroscience 18, 193-222.

1102   Fries, P. (2015). Rhythms for Cognition: Communication through Coherence. Neuron 88, 220-
1103   235.

1104   Fries, P., Reynolds, J.H., Rorie, A.E., and Desimone, R. (2001). Modulation of oscillatory
1105   neuronal synchronization by selective visual attention. Science 291, 1560-1563.

1106   Gieselmann, M.A., and Thiele, A. (2008). Comparison of spatial integration and surround
1107   suppression characteristics in spiking activity and the local field potential in macaque V1. The
1108   European journal of neuroscience 28, 447-459.

1109   Gray, C.M., König, P., Engel, A.K., and Singer, W. (1989). Oscillatory responses in cat visual
1110   cortex exhibit inter-columnar synchronization which reflects global stimulus properties. Nature
1111   338, 334-337.

1112   Gregoriou, G.G., Gotts, S.J., Zhou, H., and Desimone, R. (2009). High-frequency, long-range
1113   coupling between prefrontal and visual cortex during attention. Science 324, 1207-1210.

1114   Grothe, I., Neitzel, S.D., Mandon, S., and Kreiter, A.K. (2012). Switching neuronal inputs by
1115   differential modulations of gamma-band phase-coherence. The Journal of neuroscience : the
1116   official journal of the Society for Neuroscience 32, 16172-16180.

1117   Haider, B., Schulz, D.P., Häusser, M., and Carandini, M. (2016). Millisecond Coupling of Local
1118   Field Potentials to Synaptic Currents in the Awake Visual Cortex. Neuron 90, 35-42.

1119   Hasenstaub, A., Shu, Y., Haider, B., Kraushaar, U., Duque, A., and McCormick, D.A. (2005).
1120   Inhibitory postsynaptic potentials carry synchronized frequency information in active cortical
1121   networks. Neuron 47, 423-435.

1122   Henrie, J.A., and Shapley, R. (2005). LFP power spectra in V1 cortex: the graded effect of
1123   stimulus contrast. Journal of neurophysiology 94, 479-490.

Spyropoulos et al., Gamma-cycle amplitude versus duration in macaque visual cortex

1124 Jia, X., Smith, M.A., and Kohn, A. (2011). Stimulus selectivity and spatial coherence of gamma
1125 components of the local field potential. The Journal of neuroscience : the official journal of the
1126 Society for Neuroscience 31, 9390-9403.

1127 Jia, X., Tanabe, S., and Kohn, A. (2013a). gamma and the coordination of spiking activity in
1128 early visual cortex. Neuron 77, 762-774.

1129 Jia, X., Xing, D., and Kohn, A. (2013b). No consistent relationship between gamma power and
1130 peak frequency in macaque primary visual cortex. The Journal of neuroscience : the official
1131 journal of the Society for Neuroscience 33, 17-25.

1132 Lewis, C.M., Bosman, C.A., Womelsdorf, T., and Fries, P. (2016). Stimulus-induced visual
1133 cortical networks are recapitulated by spontaneous local and interareal synchronization.
1134 Proceedings of the National Academy of Sciences of the United States of America 113, E606-
1135 615.

1136 Lima, B., Singer, W., Chen, N.H., and Neuenschwander, S. (2010). Synchronization dynamics
1137 in response to plaid stimuli in monkey V1. Cereb Cortex 20, 1556-1573.

1138 Lowet, E., Gips, B., Roberts, M.J., De Weerd, P., Jensen, O., and van der Eerden, J. (2018).
1139 Microsaccade-rhythmic modulation of neural synchronization and coding within and across
1140 cortical areas V1 and V2. PLoS biology 16, e2004132.

1141 Lowet, E., Roberts, M.J., Bosman, C.A., Fries, P., and De Weerd, P. (2016). Areas V1 and V2
1142 show microsaccade-related 3-4-Hz covariation in gamma power and frequency. The European
1143 journal of neuroscience 43, 1286-1296.

1144 Lowet, E., Roberts, M.J., Peter, A., Gips, B., and De Weerd, P. (2017). A quantitative theory of
1145 gamma synchronization in macaque V1. eLife 6.

1146 Lundqvist, M., Rose, J., Herman, P., Brincat, S.L., Buschman, T.J., and Miller, E.K. (2016).
1147 Gamma and Beta Bursts Underlie Working Memory. Neuron 90, 152-164.

1148 Mann, E.O., Suckling, J.M., Hajos, N., Greenfield, S.A., and Paulsen, O. (2005). Perisomatic
1149 feedback inhibition underlies cholinergically induced fast network oscillations in the rat
1150 hippocampus in vitro. Neuron 45, 105-117.

1151 Mitchell, J.F., Sundberg, K.A., and Reynolds, J.H. (2007). Differential attention-dependent
1152 response modulation across cell classes in macaque visual area V4. Neuron 55, 131-141.

1153 Muller, L., Reynaud, A., Chavane, F., and Destexhe, A. (2014). The stimulus-evoked population
1154 response in visual cortex of awake monkey is a propagating wave. Nature communications 5,
1155 3675.

1156 Okun, M., and Lampl, I. (2008). Instantaneous correlation of excitation and inhibition during
1157 ongoing and sensory-evoked activities. Nature neuroscience 11, 535-537.

1158 Onorato, I., Neuenschwander, S., Hoy, J.L., Lima, B., Rocha, S., Broggini, A.C., Uran, C.,
1159 Spyropoulos, G., Womelsdorf, T., Fries, P.*, et al.* (2019). A distinct class of bursting neurons
1160 with strong gamma synchronization and stimulus selectivity in monkey V1. Neuron (in press).

Spyropoulos et al., Gamma-cycle amplitude versus duration in macaque visual cortex

1161 Oostenveld, R., Fries, P., Maris, E., and Schoffelen, J.M. (2011). FieldTrip: Open source
1162 software for advanced analysis of MEG, EEG, and invasive electrophysiological data.
1163 Computational intelligence and neuroscience 2011, 156869.

1164 Palmigiano, A., Geisel, T., Wolf, F., and Battaglia, D. (2017). Flexible information routing by
1165 transient synchrony. Nature neuroscience 20, 1014-1022.

1166 Pesaran, B., Pezaris, J.S., Sahani, M., Mitra, P.P., and Andersen, R.A. (2002). Temporal
1167 structure in neuronal activity during working memory in macaque parietal cortex. Nature
1168 neuroscience 5, 805-811.

1169 Peter, A., Uran, C., Klon-Lipok, J., Roese, R., van Stijn, S., Barnes, W., Dowdall, J.R., Singer,
1170 W., Fries, P., and Vinck, M. (2019). Surface color and predictability determine contextual
1171 modulation of V1 firing and gamma oscillations. eLife 8.

1172 Ray, S., and Maunsell, J.H. (2010). Differences in gamma frequencies across visual cortex
1173 restrict their possible use in computation. Neuron 67, 885-896.

1174 Reynolds, J.H., Chelazzi, L., and Desimone, R. (1999). Competitive mechanisms subserve
1175 attention in macaque areas V2 and V4. The Journal of neuroscience : the official journal of the
1176 Society for Neuroscience 19, 1736-1753.

1177 Roberts, M.J., Lowet, E., Brunet, N.M., Ter Wal, M., Tiesinga, P., Fries, P., and De Weerd, P.
1178 (2013). Robust gamma coherence between macaque V1 and V2 by dynamic frequency
1179 matching. Neuron 78, 523-536.

1180 Rohenkohl, G., Bosman, C.A., and Fries, P. (2018). Gamma Synchronization between V1 and
1181 V4 Improves Behavioral Performance. Neuron 100, 953-963 e953.

1182 Rubehn, B., Bosman, C., Oostenveld, R., Fries, P., and Stieglitz, T. (2009). A MEMS-based
1183 flexible multichannel ECoG-electrode array. Journal of neural engineering 6, 036003.

1184 Salkoff, D.B., Zagha, E., Yüzgeç, O., and McCormick, D.A. (2015). Synaptic Mechanisms of
1185 Tight Spike Synchrony at Gamma Frequency in Cerebral Cortex. The Journal of neuroscience :
1186 the official journal of the Society for Neuroscience 35, 10236-10251.

1187 Schmitzer-Torbert, N., Jackson, J., Henze, D., Harris, K., and Redish, A.D. (2005). Quantitative
1188 measures of cluster quality for use in extracellular recordings. Neuroscience 131, 1-11.

1189 Shirhatti, V., and Ray, S. (2018). Long-wavelength (reddish) hues induce unusually large
1190 gamma oscillations in the primate primary visual cortex. Proceedings of the National Academy
1191 of Sciences of the United States of America 115, 4489-4494.

1192 Shu, Y., Hasenstaub, A., and McCormick, D.A. (2003). Turning on and off recurrent balanced
1193 cortical activity. Nature 423, 288-293.

1194 Siegle, J.H., Pritchett, D.L., and Moore, C.I. (2014). Gamma-range synchronization of fast-
1195 spiking interneurons can enhance detection of tactile stimuli. Nature neuroscience 17, 1371-
1196 1379.

Spyropoulos et al., Gamma-cycle amplitude versus duration in macaque visual cortex

1197   Tiesinga, P., and Sejnowski, T.J. (2009). Cortical enlightenment: are attentional gamma
1198   oscillations driven by ING or PING? Neuron 63, 727-732.

1199   Tiesinga, P.H., Fellous, J.M., Jose, J.V., and Sejnowski, T.J. (2001). Computational model of
1200   carbachol-induced delta, theta, and gamma oscillations in the hippocampus. Hippocampus 11,
1201   251-274.

1202   Traub, R.D., Jefferys, J.G., and Whittington, M.A. (1997). Simulation of gamma rhythms in
1203   networks of interneurons and pyramidal cells. Journal of computational neuroscience 4, 141-
1204   150.

1205   Traub, R.D., Whittington, M.A., Colling, S.B., Buzsáki, G., and Jefferys, J.G. (1996). Analysis of
1206   gamma rhythms in the rat hippocampus in vitro and in vivo. The Journal of physiology 493 (Pt
1207   2), 471-484.

1208   Vinck, M., Battaglia, F.P., Womelsdorf, T., and Pennartz, C. (2012). Improved measures of
1209   phase-coupling between spikes and the Local Field Potential. Journal of computational
1210   neuroscience 33, 53-75.

1211   Vinck, M., and Bosman, C.A. (2016). More Gamma More Predictions: Gamma-Synchronization
1212   as a Key Mechanism for Efficient Integration of Classical Receptive Field Inputs with Surround
1213   Predictions. Frontiers in systems neuroscience 10, 35.

1214   Vinck, M., Lima, B., Womelsdorf, T., Oostenveld, R., Singer, W., Neuenschwander, S., and
1215   Fries, P. (2010a). Gamma-phase shifting in awake monkey visual cortex. The Journal of
1216   neuroscience : the official journal of the Society for Neuroscience 30, 1250-1257.

1217   Vinck, M., van Wingerden, M., Womelsdorf, T., Fries, P., and Pennartz, C.M. (2010b). The
1218   pairwise phase consistency: A bias-free measure of rhythmic neuronal synchronization.
1219   NeuroImage 51, 112-122.

1220   Vinck, M., Womelsdorf, T., Buffalo, E.A., Desimone, R., and Fries, P. (2013a). Attentional
1221   modulation of cell-class-specific gamma-band synchronization in awake monkey area V4.
1222   Neuron 80, 1077-1089.

1223   Vinck, M., Womelsdorf, T., and Fries, P. (2013b). Gamma oscillations and information
1224   transmission. In Principles of Neural Coding
1225   R.Q. Quiroga, and S. Panzeri, eds. (CRC Press).

1226   Wang, P., and Nikolić, D. (2011). An LCD Monitor with Sufficiently Precise Timing for Research
1227   in Vision. Frontiers in human neuroscience 5, 85.

1228   Wehr, M., and Zador, A.M. (2003). Balanced inhibition underlies tuning and sharpens spike
1229   timing in auditory cortex. Nature 426, 442-446.

1230   Whittington, M.A., Traub, R.D., and Jefferys, J.G. (1995). Synchronized oscillations in
1231   interneuron networks driven by metabotropic glutamate receptor activation. Nature 373, 612-
1232   615.

1233   Whittington, M.A., Traub, R.D., Kopell, N., Ermentrout, B., and Buhl, E.H. (2000). Inhibition-
1234   based rhythms: experimental and mathematical observations on network dynamics.

Spyropoulos et al., Gamma-cycle amplitude versus duration in macaque visual cortex

1235 International journal of psychophysiology : official journal of the International Organization of
1236 Psychophysiology 38, 315-336.

1237 Womelsdorf, T., and Fries, P. (2007). The role of neuronal synchronization in selective attention.
1238 Current opinion in neurobiology 17, 154-160.

1239 Womelsdorf, T., Lima, B., Vinck, M., Oostenveld, R., Singer, W., Neuenschwander, S., and
1240 Fries, P. (2012). Orientation selectivity and noise correlation in awake monkey area V1 are
1241 modulated by the gamma cycle. Proceedings of the National Academy of Sciences of the United
1242 States of America 109, 4302-4307.

1243 Zheng, C., Bieri, K.W., Hsiao, Y.T., and Colgin, L.L. (2016). Spatial Sequence Coding Differs
1244 during Slow and Fast Gamma Rhythms in the Hippocampus. Neuron 89, 398-408.
1245
1246

Spyropoulos et al., Gamma-cycle amplitude versus duration in macaque visual cortex
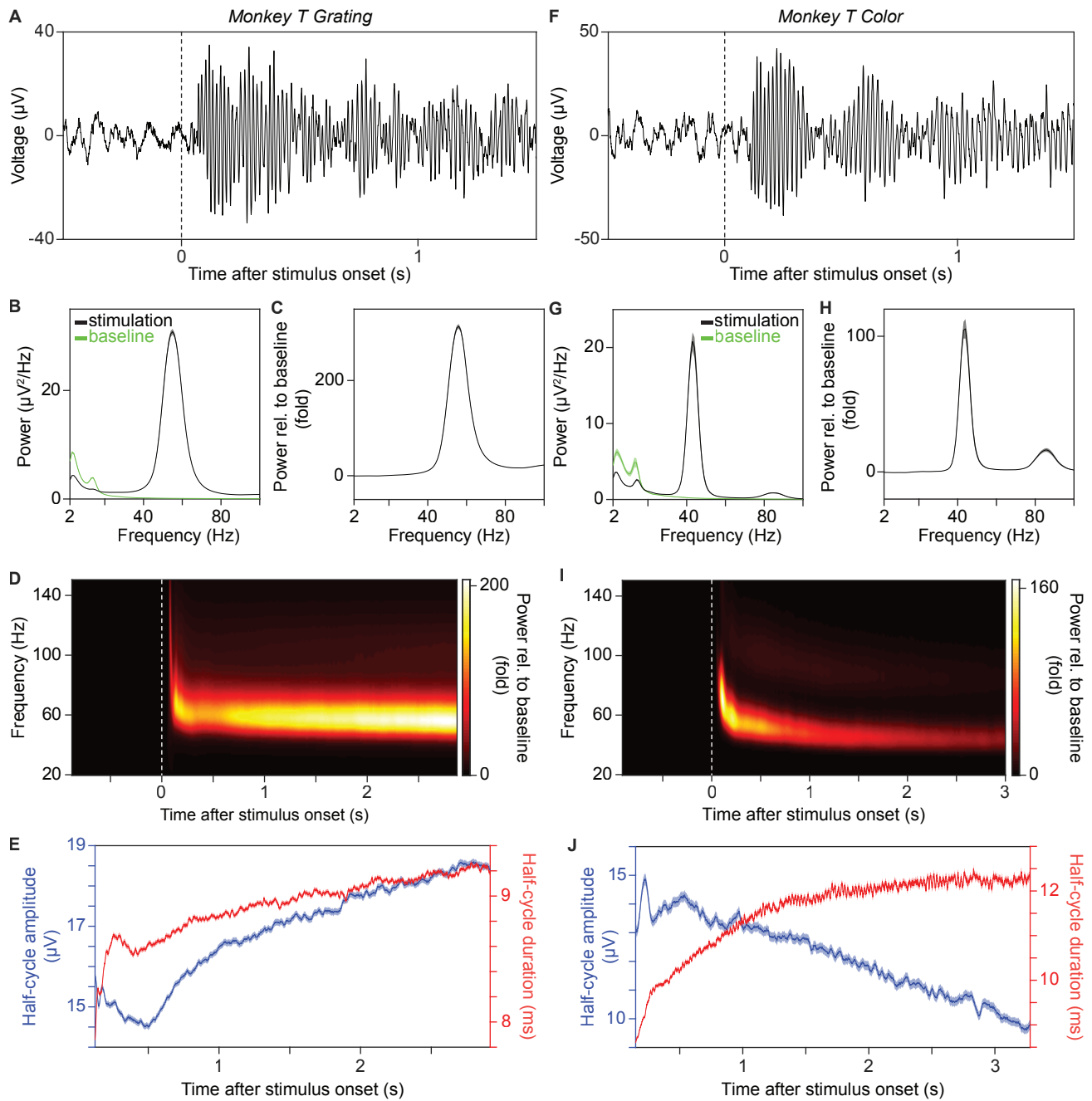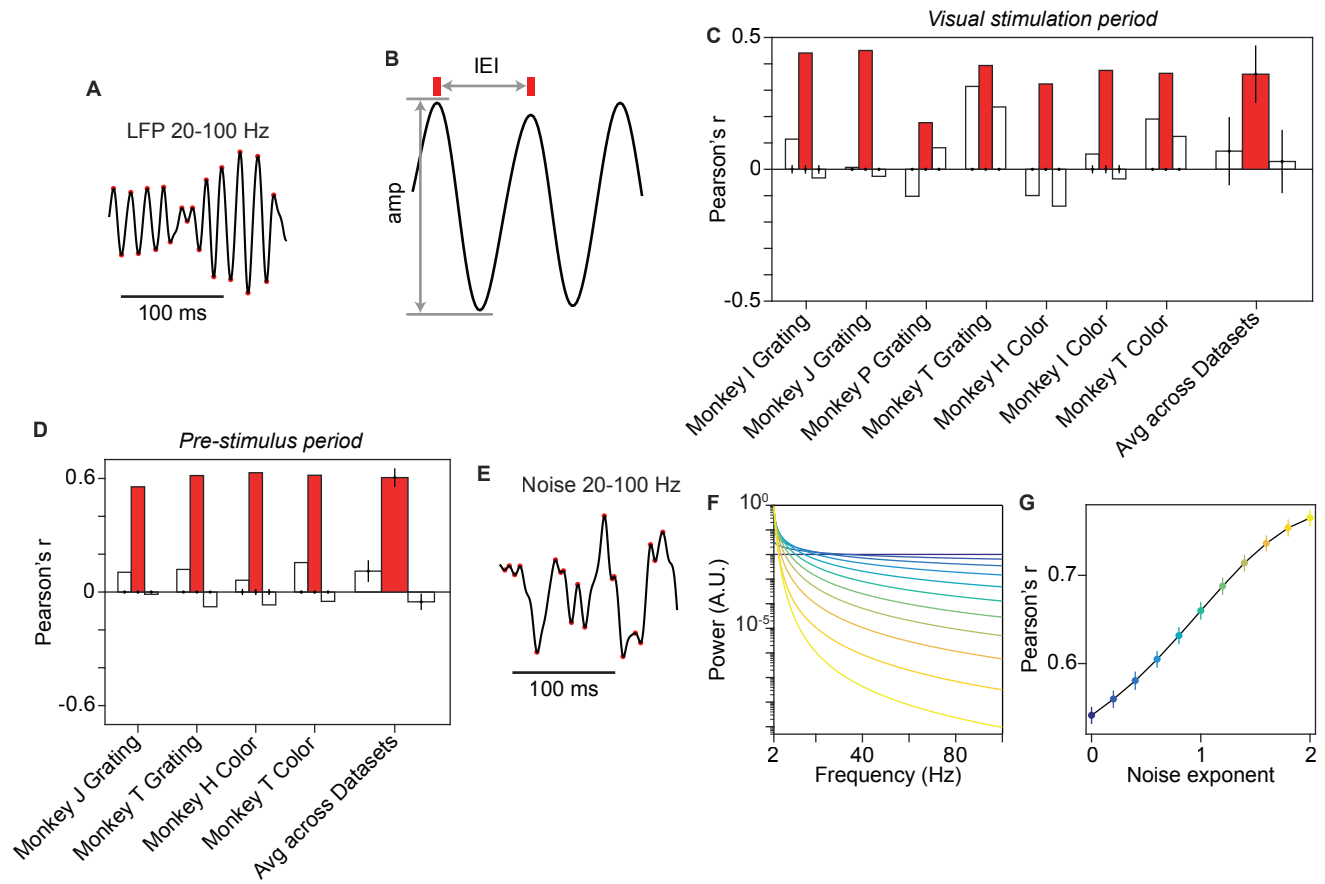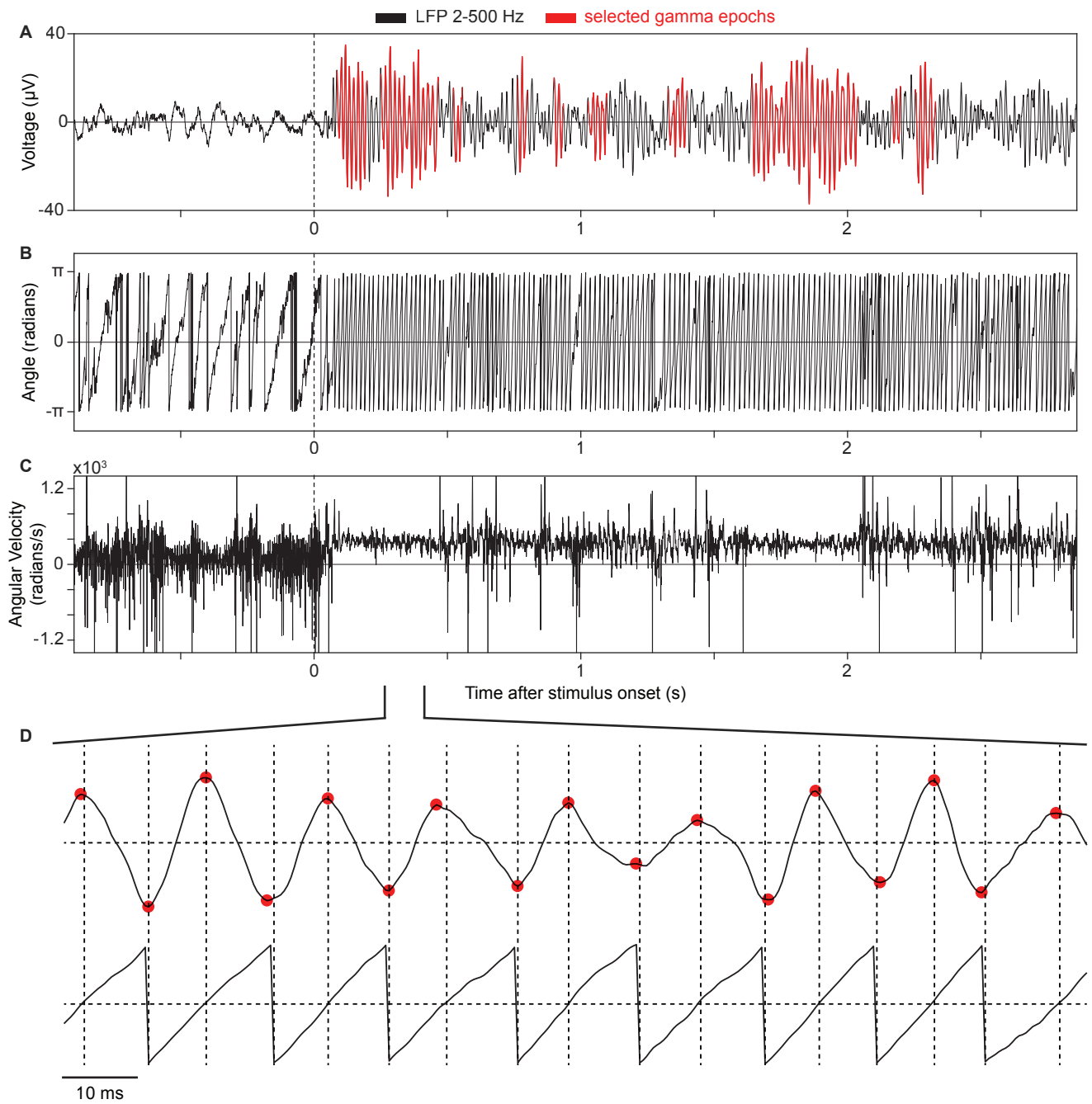
Figure 1

Figure 2

Figure 3
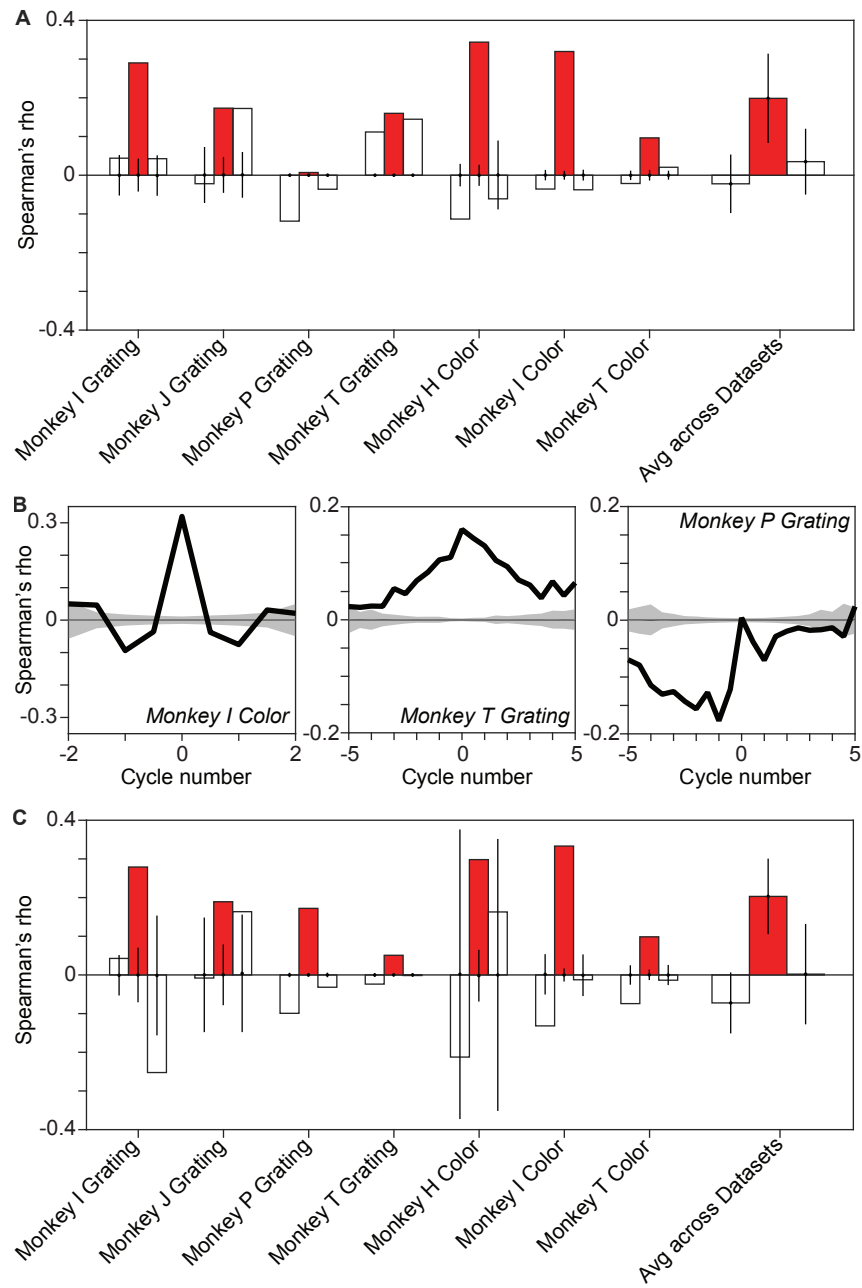
Figure 4
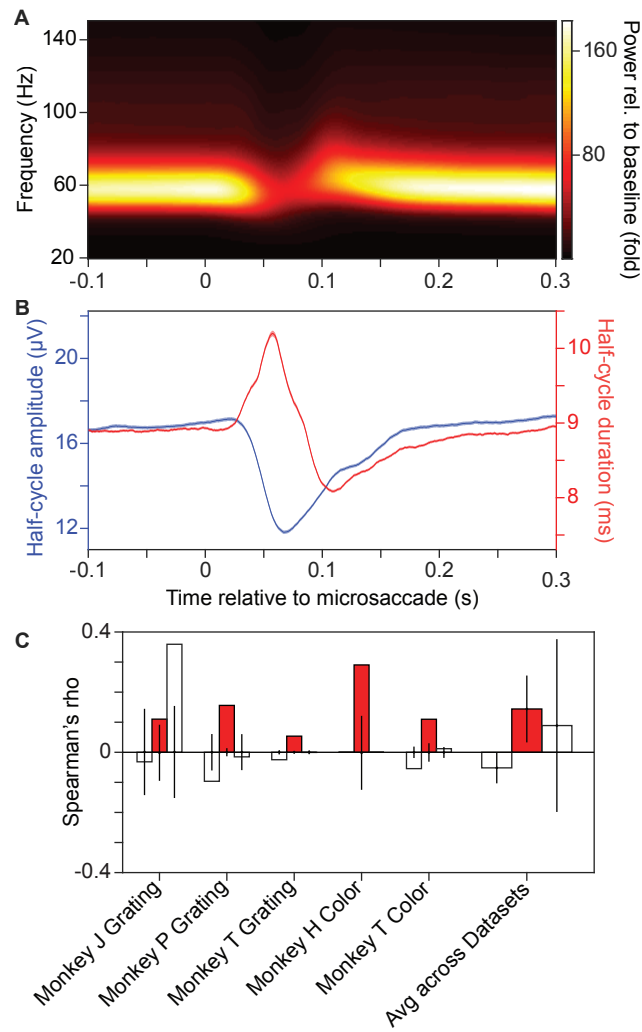
Figure 5

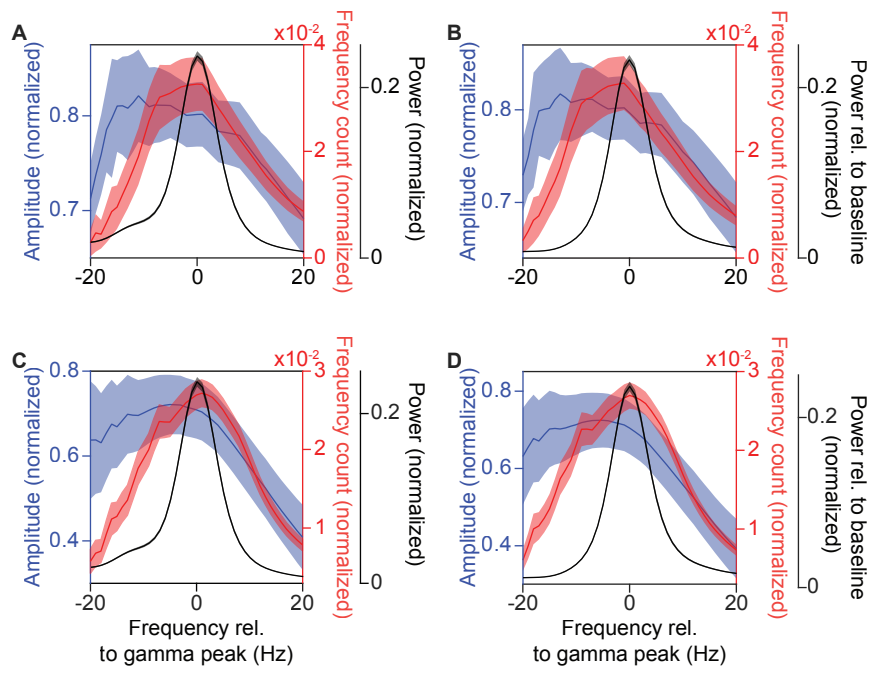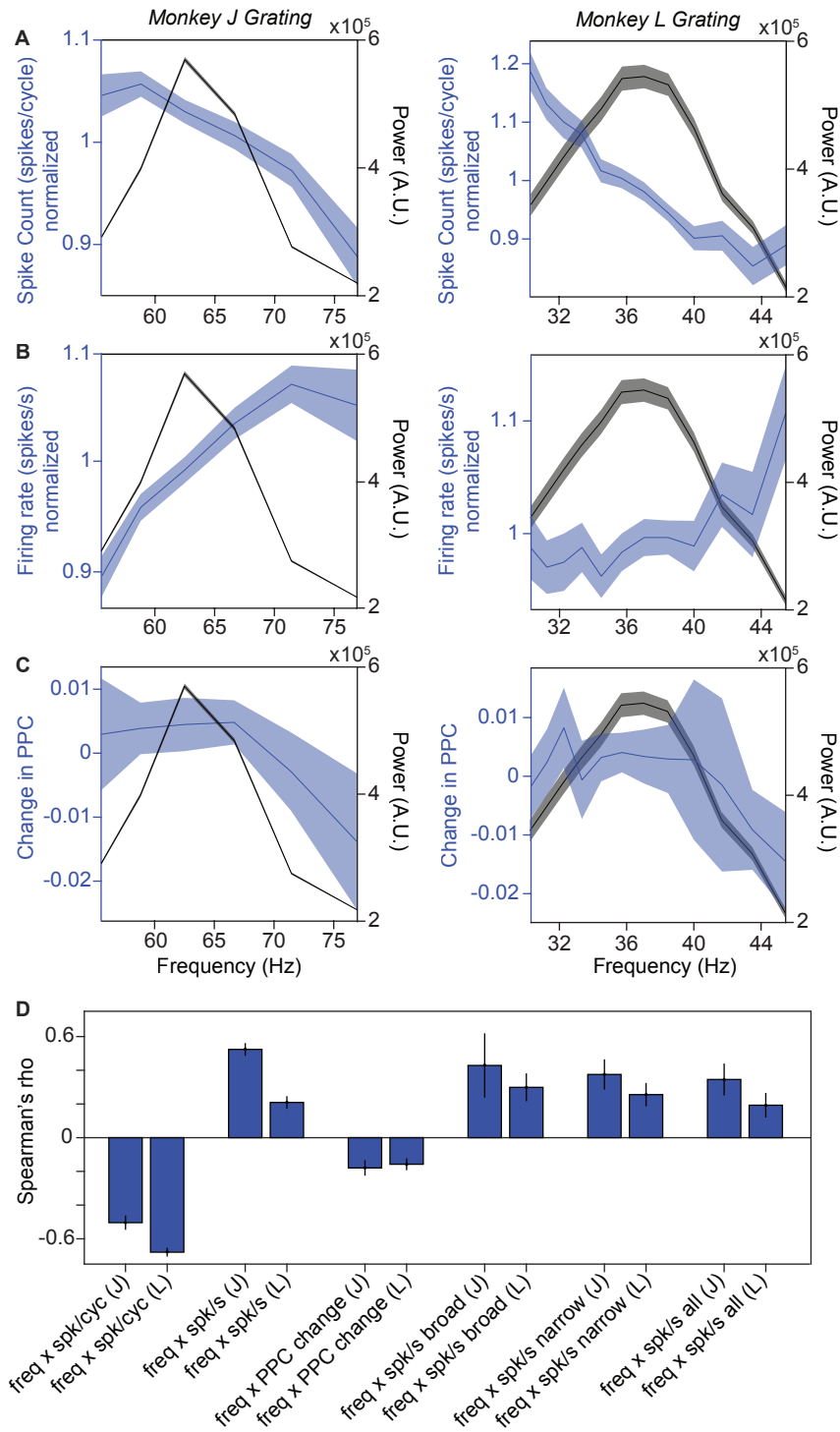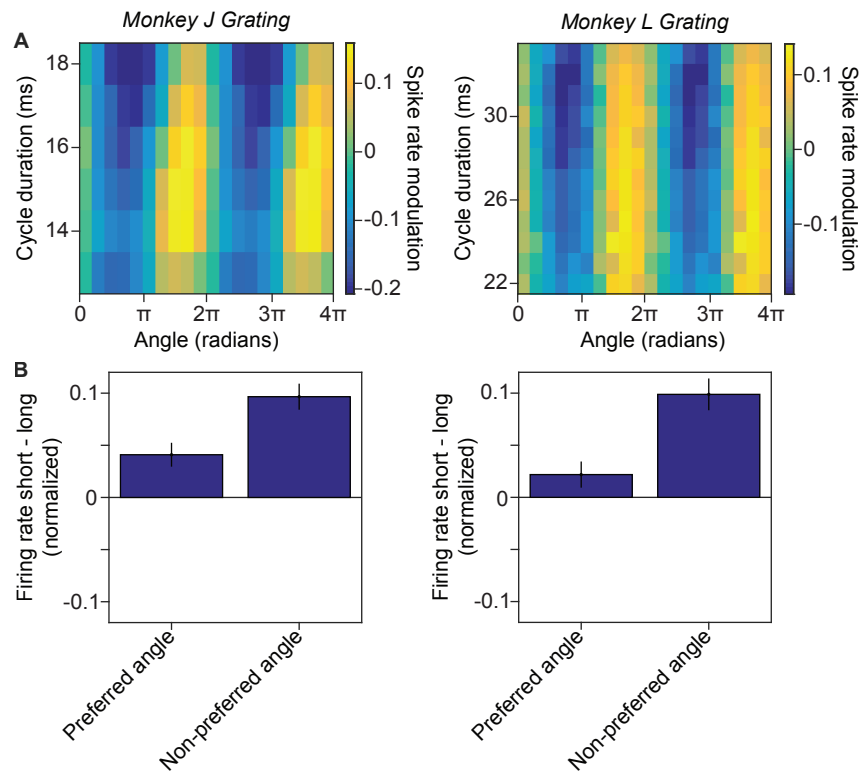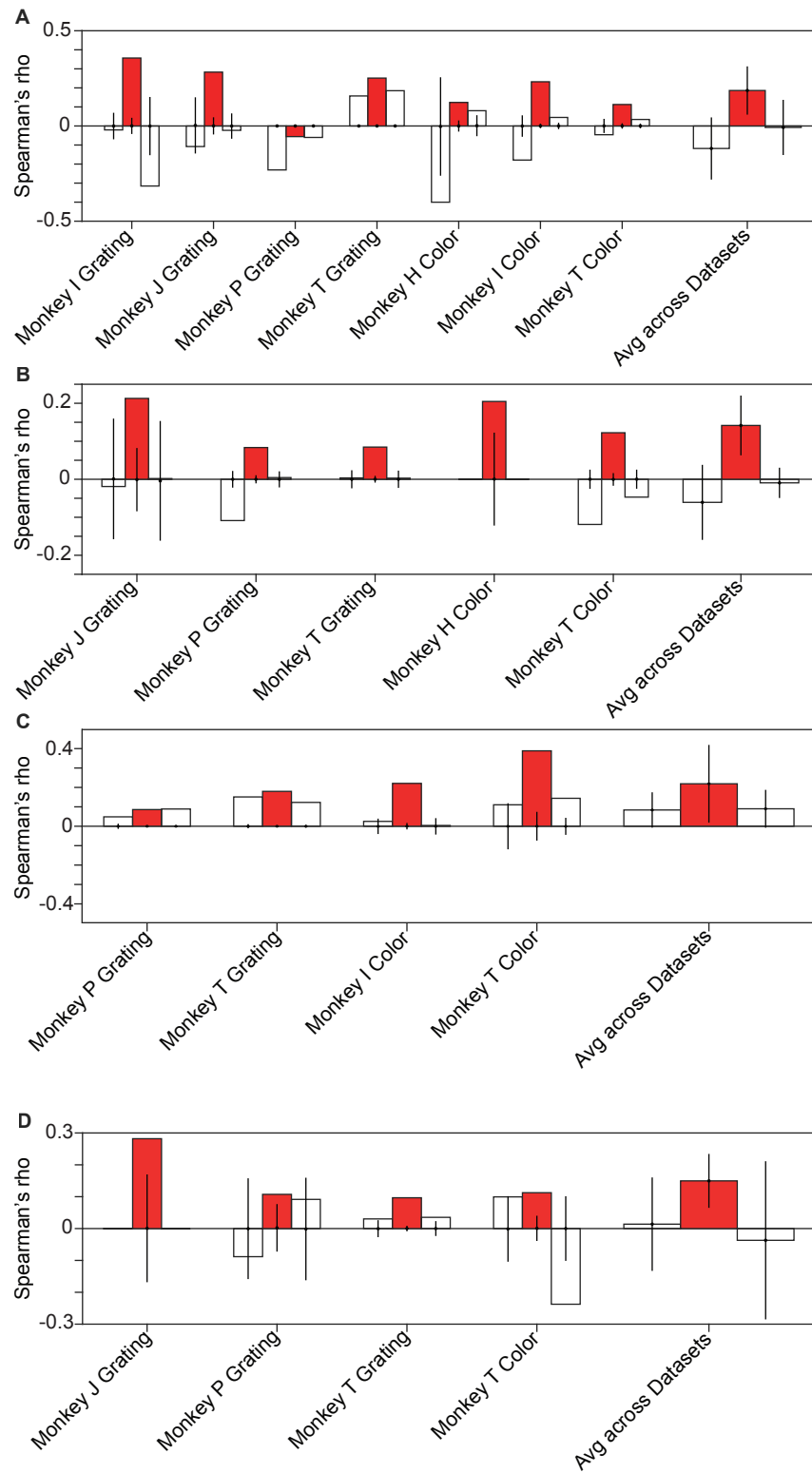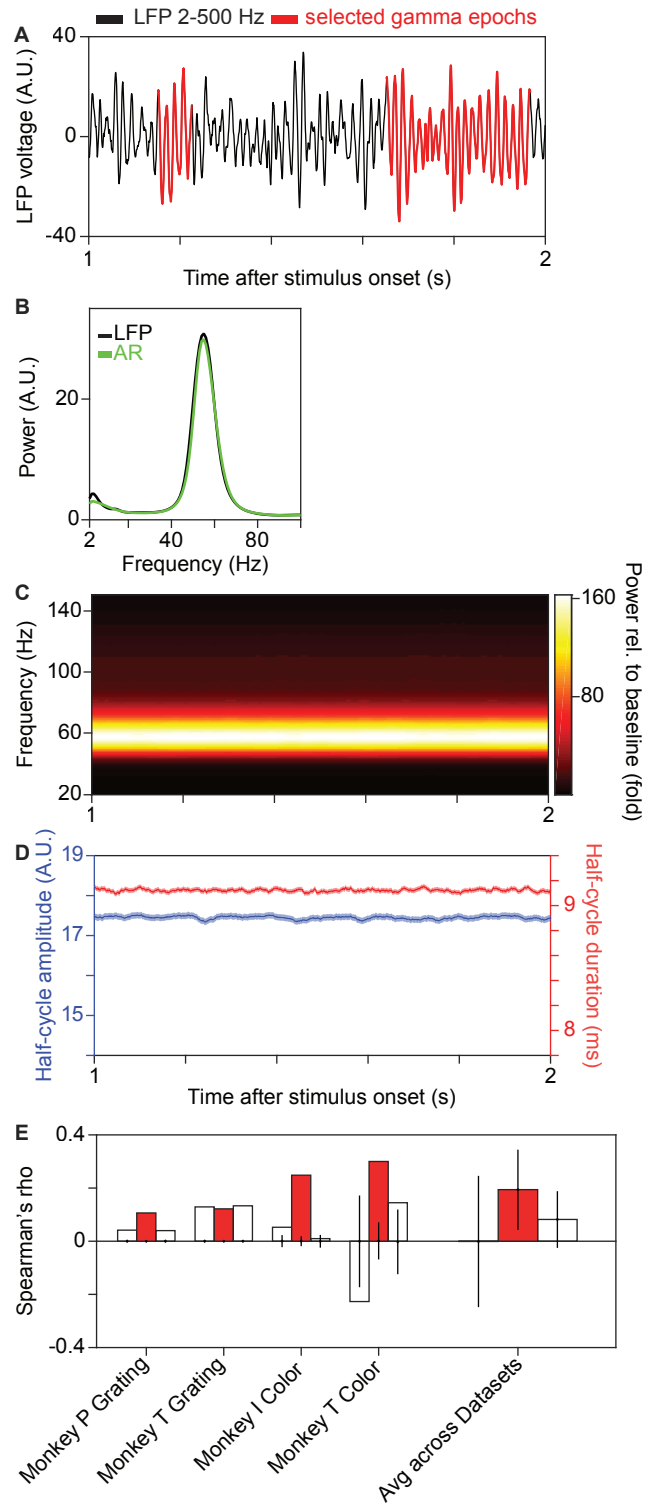Figure 6

Figure 7

Figure 8

Supplementary Figure 1

Supplementary Figure 2